



1 **Retrogressive thaw slumps temper dissolved organic carbon delivery to streams of the Peel Plateau,**  
2 **NWT, Canada**

3

4 Cara A. Bulger<sup>1\*</sup>, Suzanne E. Tank<sup>1</sup>, and Steven V. Kokelj<sup>2</sup>

5

6 <sup>1</sup>Department of Biological Sciences, University of Alberta, Edmonton, AB, Canada, T6G 2E9

7 <sup>2</sup>Northwest Territories Geological Survey, Government of the Northwest Territories, Yellowknife, NT,  
8 Canada

9 \*Author for correspondence: [cara.bulger@gmail.com](mailto:cara.bulger@gmail.com)

10

11



## 12 Abstract

13 In Siberia and Alaska, permafrost thaw has been associated with significant increases in the delivery of  
14 dissolved organic carbon (DOC) to recipient stream ecosystems. Here, we examine the effect of  
15 retrogressive thaw slumps (RTS) on DOC concentration and transport, using data from eight RTS features  
16 on the Peel Plateau, NT, Canada. Like extensive regions of northwestern Canada, the Peel Plateau is  
17 comprised of thick, ice-rich tills that were deposited at the margins of the **continental ice sheet**. RTS  
18 features are now widespread in this region, with headwall exposures up to 30 m high, and total  
19 disturbed areas often exceeding 30 ha. We find that intensive slumping on the Peel Plateau is universally  
20 associated with decreasing DOC concentrations downstream of slumps, even though the composition of  
21 slump-derived dissolved organic matter (DOM; assessed using specific UV absorbance and slope ratios)  
22 is similar to permafrost-derived DOM from other regions. Comparisons of upstream and downstream  
23 DOC flux relative to a conservative **tracer** suggest that the substantial fine-grained sediments released  
24 by slumping may **sequester DOC on this landscape**. **Runoff obtained directly from within slump features,**  
25 **above entry into recipient streams, indicates that the deepest RTS features, which thaw the greatest**  
26 **extent of buried, Pleistocene-aged glacial tills, have the lowest runoff DOC concentrations when**  
27 **compared to upstream, un-disturbed locations**. In contrast, shallower features, with exposures that are  
28 more limited to a relict Holocene active layer, have within-slump DOC concentrations more similar to  
29 upstream sites. Finally, fine-scale work at a single RTS feature indicates that temperature and  
30 precipitation serve as primary environmental controls on above-slump and below-slump DOC flux, but  
31 that the relationship between climatic parameters and DOC flux is complex for these dynamic  
32 thermokarst features. These results demonstrate that we should expect striking variation in  
33 thermokarst-associated DOC mobilization across Arctic regions, but that within-region variation in  
34 thermokarst intensity and other landscape factors are also important for determining biogeochemical  
35 response. An understanding of landscape and climate history, permafrost genesis, soil composition, the  
36 nature and intensity of thermokarst, and the interaction of these factors, is critical for predicting



37 changes in land-to-water carbon mobilization in a warming **circumpolar world**.

38

39

## 40 **1. Introduction**

41 Anthropogenic climate change is significantly affecting the Canadian Arctic cryosphere (IPCC,  
42 2014). Temperature increases in Arctic regions are predicted to be at least 40% greater than the global  
43 mean (IPCC, 2014), while **precipitation is also expected to increase significantly** (Walsh et al., 2011). The  
44 resulting degradation of permafrost is **forecast** to have wide-ranging effects, because thawing has the  
45 potential to greatly alter the physical, chemical, and biological functioning of landscapes (Frey and  
46 McClelland, 2009; Khvorostyanov et al., 2008a, 2008b; Kokelj et al., 2017b; Schuur et al., 2008, 2013). In  
47 particular, permafrost acts as a long term storage medium for solutes and sediments, and as a barrier to  
48 the participation of permafrost-sequestered constituents within active biogeochemical cycles (McGuire  
49 et al., 2009). Consequently, permafrost thaws enhances linkages between terrestrial and aquatic  
50 systems, via increasing transport of terrestrial compounds from land to water (Kokelj et al. 2013; Tanski  
51 et al., 2016; Vonk et al., 2015b). Given that **global permafrost** stores of carbon are estimated to be  
52 almost double that of the atmospheric carbon pool (Hugelius et al., 2014), there is great potential for  
53 large increases in carbon mobilization as a result of permafrost thaw (Schuur et al., 2015). Within this  
54 context, the transport of dissolved organic carbon (DOC) from land to water is of particular interest,  
55 because DOC acts as the primary substrate for the microbially-mediated mineralization of organic  
56 carbon to carbon dioxide (Battin et al., 2008; Spencer et al., 2015). **Dissolved organic carbon** also forms  
57 the majority of total organic carbon flux in most Arctic rivers (Spencer et al., 2015), and is thus the  
58 primary vehicle for the delivery of terrestrial carbon to the Arctic Ocean (Dittmar and Kattner, 2003;  
59 Holmes et al., 2012). As a result, the implications of thaw-mediated DOC mobilization may range from  
60 effects on the permafrost-carbon feedback, to the ecological and biogeochemical functioning of  
61 streams, rivers, and the **nearshore ocean** (e.g. Tank et al., 2012b; Vonk et al., 2015b).



62 Permafrost thaw can manifest in many different forms, ranging from an increase in active layer  
63 thickness and terrain subsidence, to thermokarst features that significantly reconfigure the physical  
64 structure of the landscape. Of these, thermokarst has the potential to rapidly expose significant  
65 quantities of previously-frozen soils to biological and chemical processing (Abbott et al., 2014, 2015;  
66 Kokelj and Jorgenson, 2013; Malone et al., 2013). One of the most conspicuous manifestations of  
67 thermokarst is the retrogressive thaw slump (RTS), which develops in ice-rich glacial deposits across  
68 northwestern Canada, Alaska, and western Siberia (Kokelj et al., 2017b), and in Yedoma regions of  
69 Alaska and Siberia (Murton et al., 2017). Thaw slumps are widespread throughout glaciated terrain in  
70 the western Canadian Arctic (Kokelj et al., 2017b), including on the Peel Plateau (Lacelle et al., 2015).  
71 These dynamic landforms develop via the ablation of an ice-rich headwall and – through the coupling of  
72 geomorphic and thermal processes – are particularly efficient at thawing thick zones of ice-rich  
73 permafrost and translocating large volumes of sediment from slopes to downstream environments (see  
74 Fig. 1). RTS features remain active for decades. They typically stabilize following sediment accumulation  
75 at the base of the headwall that insulates the ground ice and arrests thaw (Kokelj et al., 2015), but can  
76 reactivate causing thaw within the scar zone, and upslope expansion of the disturbance (Kokelj et al.,  
77 2013; Lantuit and Pollard, 2008). During periods of activity, thawed materials accumulate as a saturated  
78 slurry in the slump scar zone (see Fig. 1b) and are translocated downslope by mass flow processes,  
79 which are accelerated by meltwater- and rainfall-induced saturation (Kokelj et al. 2015). During active  
80 and stabilized periods, surface runoff can also remove solutes and suspended sediment from the  
81 thawed substrate to downstream environments. Although variation in temperature, precipitation and  
82 solar radiation have been correlated with development rates and growth of retrogressive thaw slumps  
83 (Kokelj et al., 2009, 2013, 2015; Lacelle et al., 2010; Lewkowicz, 1986, 1987), we know little about how  
84 these and other environmental drivers might control permafrost-DOC dynamics at the individual-slump  
85 to small watershed scale.



86           On the Peel Plateau, individual thaw slumps commonly impact tens of hectares of terrain,  
87   displace hundreds of thousands of cubic meters of sediments downslope, and significantly alter surface  
88   water sediment and solute loads (Kokelj et al., 2013; Malone et al., 2013), and thus downstream  
89   ecosystems (Chin et al., 2016; Malone et al., 2013). The magnitude of these disturbances and their  
90   cumulative impacts is great enough to alter solute loads in the Peel River (70,000 km<sup>2</sup> watershed area;  
91   Kokelj et al., 2013), even though only a small portion of the river's total catchment area (<1%) is  
92   influenced by thermokarst (Kokelj et al., 2017b; Segal et al., 2016). This contrasts with many other  
93   permafrost-affected regions, where increases in solute loads following permafrost disturbance can be  
94   transient (e.g., limited to spring freshet) and have little overall effect on annual solute fluxes (for  
95   example, in High Arctic regions affected by active layer detachments; Lafrenière & Lamoureux, 2013). In  
96   addition, permafrost thaw on the Peel Plateau is notable in that it exposes vast quantities of mineral-  
97   rich glacial till, which is overlain by a relatively shallow layer of slightly more organic-rich soils (Duk-  
98   Rodkin and Hughes, 1992; Kokelj et al. 2017a). Although this landscape type is found across glaciated  
99   permafrost terrains of the circumpolar North (e.g., Kokelj et al. 2017b), it contrasts with regions of  
100   Alaska and eastern Siberia that are either Yedoma-rich or were patchily glaciated during the late  
101   Pleistocene, and which have been common focus points for study of permafrost-DOC interactions to  
102   date (Abbott et al., 2014, 2015; Drake et al., 2015; Mann et al., 2012; Vonk et al., 2013b).

103           In several Arctic regions, permafrost thaw, including thermokarst, has been documented to  
104   enhance DOC concentrations in recipient aquatic ecosystems (Frey and McClelland, 2009; Tank et al.,  
105   2012a; Vonk et al., 2013a; Vonk and Gustafsson, 2013). For example, streams draining thaw slumps have  
106   higher DOC concentrations than un-affected systems across various terrain types in Alaska (2-3 fold  
107   increase; Abbot et al., 2014), while the DOC concentration in runoff from thawing Yedoma in eastern  
108   Siberia is considerably greater than concentrations in recipient river systems (~30-fold elevation;  
109   Spencer et al. 2015). However, multiple factors, including variable carbon content in permafrost soils  
110   (Hugelis et al. 2014) may affect DOC release with permafrost thaw. In regions where thermokarst



111 transports fine-grained sediments to aquatic systems, sorption processes may also be important,  
112 because dissolved organic matter (DOM) can readily sorb to mineral [soils](#). This rapid process is largely  
113 regulated by the chemical composition and clay content of mineral sediments (Kothawala et al. 2009),  
114 and can cause DOM to be rapidly removed from solution in stream systems (Kaiser and Guggenberger,  
115 2000; McDowell, 1985). The DOM-mineral complex can be an important mechanism for enabling the  
116 downstream transport and continued sequestration of organic carbon (Hedges et al., 1997). Sorption  
117 processes may be particularly important for DOC transport in the glaciated western Canadian Arctic,  
118 where landscape predisposition to thaw slumping results in an abundance of thermokarst related slope  
119 disturbances which effectively mobilize fine-grained glacial sediment stores to downstream systems  
120 (Kokelj et al., 2017a, 2017b; Rampton, 1988).

121 In this study, we quantify how RTS features on the Peel Plateau affect the concentration and  
122 composition of DOC within a series of recipient stream systems, to explore how DOC mobilization from  
123 land to [water](#) is affected by thermokarst in this region. We further investigate how short-term variation  
124 in precipitation, temperature, and solar radiation affect DOC flux above and below a single RTS feature,  
125 to explore the drivers of temporal variation in DOC flux. We specifically target these thermokarst-  
126 sensitive glacial deposits, which are characteristic of large portions of the circumpolar Arctic, to explicitly  
127 consider how variations in permafrost soil composition, permafrost genesis, and Quaternary history,  
128 influence variability in permafrost-DOC interactions across vast Arctic regions. **The study results broaden  
129 our understanding of land-water carbon mobilization in permafrost terrain, and indicate that slumping  
130 on the Peel Plateau may act to temper the flux of DOC within this landscape, via mineral-carbon  
131 interactions. These findings also underline the importance of landscape characteristics and geological  
132 inheritance for determining the biogeochemical effects of thermokarst, particularly as hillslope  
133 thermokarst intensifies across many Arctic regions (Kokelj et al., 2017b).**

134

135



## 136 **2 Study Site**

### 137 *2.1 General study site description*

138 Our study was conducted on the Peel Plateau, situated in the eastern foothills of the Richardson  
139 Mountains, NWT, Canada, in the zone of continuous permafrost (Fig. 1a) (Kokelj et al., 2016). The  
140 fluviially-incised Plateau ranges in elevation from 100 to 650 masl (Catto, 1996). The region was covered  
141 by the Laurentian Ice Sheet (LIS) for a brief period 18,500 cal yr BP (Lacelle et al., 2013). The bedrock of  
142 the region is Lower Cretaceous marine shale from the Arctic River formation (Norris, 1984) and siltstone  
143 overlain by Late Pleistocene glacial, glacio-fluvial and glacio-lacustrine sediments (Duk-Rodkin and  
144 Hughes, 1992), covered by a shallow organic layer. These Pleistocene deposits host ice-rich permafrost.  
145 Carbon dating and <sup>18</sup>O measurements in the region have placed the age of relict ground ice in the late  
146 Pleistocene epoch (18,100 ± 60 <sup>14</sup>Cyr BP; Lacelle et al., 2013). Upper layers of permafrost thawed during  
147 the early Holocene and host younger, Holocene-aged organic materials (7890 ± 250 <sup>14</sup>Cyr BP; Lacelle et  
148 al., 2013). These are clearly delineated from deeper Pleistocene-aged permafrost by a thaw  
149 unconformity, which developed when warmer climate during the early Holocene prompted the thawing  
150 of near-surface permafrost and a regional increase in active layer thicknesses, enabling the leaching of  
151 soluble ions and integration of organic matter into these previously thawed soils (see Fig. 1c-d).  
152 Subsequent aggradation of permafrost due to gradual cooling has archived this notable stratigraphic  
153 variation in geochemistry, organic matter content, and cryostructure (Kokelj et al., 2002; Lacelle et al.,  
154 2014; Murton and French, 1994).

155 Ice-marginal glacial landscapes such as the Peel Plateau host thick layers of ice-rich  
156 sediments, and thus have a predisposed sensitivity to climate-driven thaw slump activity (Kokelj et al.,  
157 2017). On the Peel Plateau, slumping is largely constrained by the maximum extent of the LIS, because  
158 the thick layers of ice-rich permafrost necessary for RTS activity is not present beyond its glacial limits  
159 (Lacelle et al., 2015). Fluvial incision provides the topographic gradients necessary for thaw slump



160 development and RTS features are common; ranging in size from small, newly developing features,  
161 which are relatively numerous, to those greater than 20 ha, which are rare (<5% prevalence; Lacelle et  
162 al., 2015). The recent intensification of slumping on the Peel Plateau is driven in part by increasing air  
163 temperatures and summer rainfall intensity (Kokelj et al., 2015). This intensification is also increasing the  
164 thaw of the deepest layer of ice-rich, organic-poor, Pleistocene-aged glaciogenic tills that underlie this  
165 region. The pattern of abundant thaw slump development across ice-marginal glaciated permafrost  
166 landscapes extends from the Peel Plateau across the western Canadian Arctic, and persists at  
167 continental scales (Kokelj et al., 2017b).

168

## 169 2.2 Regional climate

170 The regional climate is typical of the subarctic with long, cold winters and short, cool summers.  
171 Mean annual air temperature (1981-2010) at the Fort McPherson weather station (Fig. 1a) is -7.3 °C  
172 with average summer (June-August) temperatures of 13.3 °C (Environment Canada, 2015). A warming  
173 trend of 0.77 °C per decade since 1970 has been recorded; however these increases are most apparent  
174 in the winter months (Burn and Kokelj, 2009). Our sample period spanned the thaw months of July and  
175 August; average 1981-2010 temperatures for those months, recorded at Fort McPherson, are 15.2 and  
176 11.8 °C, respectively, slightly higher than averages observed at a more elevated, centrally-located  
177 meteorological station (Fig. 1a) during our study (13.2 °C in July and 9.5 °C in August). Annual cumulative  
178 rainfall (1981-2010) at the Fort McPherson weather station averages 145.9 mm, with July and August  
179 having the highest rainfall levels at 46.4 and 39.1 mm (Environment Canada, 2015). In 2014, rainfall for  
180 July and August was 128.7 and 170.7 mm. This makes 2014 a cooler year than average, and continues  
181 the trend of increasingly wetter summers with numerous extreme rainfall events (Kokelj et al., 2015).



182

183 **3 Methods**184 *3.1 Slump site selection*

185 Eight RTS features were selected from across the study region (Fig. 1; Fig. S1; Table 1). Selected  
186 slumps possessed a debris tongue that extended to the valley bottom and directly impacted a stream  
187 system. Sampling at each slump occurred at three discrete locations: upstream, within-slump, and  
188 downstream of slump influence (Fig. 1b). Upstream sites were trunk streams that connected with the  
189 slump flow path further downstream, and were un-affected by any major geomorphic disturbance and  
190 thus representative of an undisturbed, pristine environment. Within-slump sampling locations were  
191 locations of channelized slump runoff within the scar zone or upper debris tongue. Downstream  
192 sampling locations were located below the confluence of the sampled upstream flow and all within-  
193 slump runoff paths, and were chosen to be representative of slump impact on aquatic ecosystems  
194 across the Peel Plateau landscape. In one instance (Slump HD, August 17), a fluidized flow event  
195 between sampling events saturated the scar zone and obliterated within-slump channelized surface  
196 flow. As a result, the within-slump sample taken at this site was not representative of typical  
197 channelized slump runoff that characterized all other slump sampling conditions, and has been  
198 discarded from all analyses.

199 A general classification of the slumps is difficult as these features are influenced by a diverse  
200 range of geomorphic processes that vary in intensity over time (Table 1; Fig. S1). Three of the slumps  
201 (FM4, FM2, FM3) are classified as ‘mega slumps’, characterised by areas greater than 5 ha, a headwall  
202 greater than 4 m in height, and a debris tongue that connects the slope to the valley below (Kokelj et al.,  
203 2013, 2015). Of these, FM4 possesses a ~~substantial~~ headwall approximately 20 m in height, but is  
204 currently largely stabilized, indicated by the small outflow, long, dry, and significantly revegetated debris  
205 tongue (Fig. S1). FM2 is among the largest active slumps in the region, with a headwall 25-30 m high and  
206 visible as a much smaller feature in air photos since 1944 (Lacelle et al. 2015). FM2 geochemistry and



207 geomorphology were described by Malone et al. (2013). Slump FM3, which was chosen for our  
208 ‘environmental controls’ work (further described below) covers an area of approximately 10 ha, and has  
209 a headwall of approximately 10 m in height and a debris tongue that extends nearly 600 m down valley  
210 (Table 1). Headwall retreat rate at FM3 over a 20 year period has been calculated at  $12.5 \text{ m yr}^{-1}$  (Lacelle  
211 et al., 2015). SD is the smallest and youngest slump that we studied, and was initiated when diversion of  
212 a small creek caused lateral bank erosion. The SD headwall is 2-4 m high with a scar zone that extends  
213 approximately 20m, and no defined debris tongue. The remaining slump sites (HA, HB, HC, HD) were all  
214 well-developed active RTS features with headwalls similar to, or smaller than, FM3, but with debris  
215 tongues that are much smaller in volume (Table 1). With the exception of SD, slump headwalls exposed  
216 permafrost well below a thaw unconformity, indicating that Pleistocene-aged, unweathered glacial  
217 materials are being thawed by the slump (Lacelle et al., 2013).

218

### 219 *3.2 Field sampling and data collection*

#### 220 *3.2.1 The effect of slumping on DOC and stream water chemistry*

221 The majority of our sampling was conducted during the summer of 2014. At each slump,  
222 samples were collected at upstream, downstream, and within-slump locations. Of the eight slumps that  
223 were sampled, three were accessed from the Dempster Highway three times over the sampling season,  
224 one (FM3; see also 3.2.2) was accessed twice from the highway, and four were accessed twice via  
225 helicopter (Table 1). At each sampling location, conductivity, pH, and temperature were recorded using  
226 a YSI Pro Plus multi-parameter meter. Water samples were collected from directly below the stream  
227 surface into 1 L acid washed HDPE bottles and allowed to sit in chilled, dark conditions for 24 hours to  
228 enable the ~~substantial~~ sediments in these samples to settle out of suspension. Sample water was then  
229 filtered with pre-combusted (475°C, 4 hours) Whatman GF/F filters (0.7  $\mu\text{m}$  pore size). Filtered sample  
230 water was transferred into 40 mL acid washed, pre-combusted glass bottles for DOC analysis, or 60 mL  
231 acid washed HDPE bottles for the analysis of absorbance and major ions. DOC samples were acidified



232 with hydrochloric acid ( $1\mu\text{L mL}^{-1}$ ), following Vonk et al. (2015b). All samples were refrigerated until  
233 analysis. The GF/F filters were retained for total suspended sediment (TSS) analysis. Samples for stable  
234 water isotope analyses were collected directly from streams into acid washed 40 mL HDPE bottles with  
235 no headspace. Bottles were sealed and refrigerated until analysis. During 2016, samples were  
236 additionally collected from a subset of slump locations (FM2, FM3, FM4 and SD) for the  $^{14}\text{C}$  signature of  
237 DOC at upstream and within-slump sites. Field samples were collected in pre-washed 1-2 L  
238 polycarbonate bottles, allowed to settle for 24 hours, and filtered using pre-combusted Whatman GF/F  
239 filters into pre-combusted glass media bottles with phenolic screw caps with butyl septa. Sample bottles  
240 were wrapped in aluminum foil and refrigerated until analysis.

241

## 242 3.2.2 Environmental controls on DOC flux

243 To explore how environmental variables control the flux of DOC from RTS-affected streams, we  
244 visited slump FM3 an additional 17 times beyond the sampling described above. During each visit, we  
245 measured discharge at the upstream and downstream locations to calculate DOC flux, and collected  
246 upstream and downstream DOC concentration samples. Downstream discharge was measured using an  
247 OTT C2 current meter at three locations across the small stream and at 40% depth. Due to the shallow,  
248 low flow conditions at the upstream site, upstream discharge was measured using the cross sectional  
249 method (Ward and Robinson, 2000). In both cases, discharge was calculated as the product of velocity  
250 and stream cross-sectional area. Local daily climate data were obtained from an automated  
251 meteorological station previously established in 2010 by the Government of the Northwest Territories  
252 (Kokelj et al. 2015). The station is located within 2 km of slump FM3 (Fig. 1a) and is instrumented for the  
253 measurement of air temperature, rainfall, and net radiation.



254

### 255 3.3 Laboratory analyses

#### 256 3.3.1 Major ions, dissolved organic carbon, $\delta^{18}\text{O}$ and $\text{DO}^{14}\text{C}$

257 Cation concentrations ( $\text{Ca}^{2+}$ ,  $\text{Mg}^{2+}$ ,  $\text{Na}^{+}$ ) were analyzed on a Perkin Elmer Analyst 200 Atomic  
258 Absorption Spectrometer at York University. A subset of collected samples were analyzed for total  
259 dissolved Fe at the University of Alberta on an Inductively Coupled Plasma - Optical Emission  
260 Spectrometer (Thermo Scientific ICAP6300), to allow for the correction of our Specific UV Absorbance  
261 results (see below). DOC samples were analyzed on a Shimadzu TOC-V analyzer; DOC was calculated as  
262 the mean of the best 3 of 5 injections with a coefficient of variance of <2%. A Picarro liquid water  
263 isotope analyzer was used to measure stable water isotope samples at the University of Alberta,  
264 following filtration (0.45  $\mu\text{m}$  cellulose acetate, Sartorius) into 2 mL autosampler vials (National  
265 Scientific), without headspace. The precision of our  $\delta^{18}\text{O}$  analysis is  $\pm 0.2\%$ . The radiocarbon signature of  
266 DOC was measured following extraction and purification at the A.E. Lalonde AMS facility (University of  
267 Toronto) using a 3MV tandem accelerator mass spectrometer (High Voltage Engineering) following  
268 established methodologies (Lang et al., 2016; Palstra and Meijer, 2014; Zhou et al., 2015).

269

#### 270 3.3.2 Total suspended sediments

271 Samples for total suspended ~~sediments~~ (TSS) were filtered in the field for later analysis, ensuring  
272 that there was enough sediment on the pre-combusted (475°C, 4 hours) and pre-weighed GF/F filters.  
273 Filters were stored frozen, dried at 60°C for 8 hours, placed in a desiccator overnight and promptly  
274 weighed. TSS was calculated as the difference in filter weight before and after sediment loading, divided  
275 by volume filtered.

276

#### 277 3.3.3 Dissolved organic matter spectral characteristics

278 DOM composition was assessed using absorbance-based metrics. A 5 cm quartz cuvette was



279 used to obtain UV-visible spectra data from 250-750 nm, using a Genesys 10 UV-Vis spectrophotometer.  
280 A baseline correction was applied to eliminate potential interference from particles following Green &  
281 Blough (1994). Specific UV absorbance at 254 nm ( $SUVA_{254}$ ), which is correlated with DOM aromaticity  
282 (Weishaar and Aiken, 2003), was calculated by dividing the decadal absorbance at 254 nm ( $m^{-1}$ ) by the  
283 DOC concentration ( $mg\ L^{-1}$ ).  $SUVA_{254}$  values were corrected for Fe interference following Poulin et al.  
284 (2014) using maximum Fe concentrations from laboratory analyses or as reported in Malone et al.  
285 (2013). Spectral slopes between 275 and 295 nm, and 350 and 400 nm ( $S_{275-295}$ ,  $S_{350-400}$ ) were calculated  
286 following Helms et al. (2008), and are reported as positive values to adhere to mathematical  
287 conventions. Slope ratios ( $S_R$ ), which correlate with DOM molecular weight (Helms et al., 2008), were  
288 calculated as the ratio of  $S_{275-295}$  to  $S_{350-400}$ .

289

290 *3.4 Statistical analyses*

291 Statistical analyses were completed in R version 3.1.3 (R Core Team, 2015) using packages ‘nlme’  
292 (Pinheiro et al., 2015), ‘lme4’ (Zeileis and Hothorn, 2002), ‘lmerTest’ (Curtin, 2015), ‘car’ (Fox and  
293 Weisberg, 2011), and ‘zoo’ (Zeileis and Grothendieck, 2005). The effect of slumping on stream chemistry  
294 and optical characteristics was assessed using linear mixed effects models in the ‘nlme’ package of R. For  
295 each parameter, analyses were split into two separate models that included data for upstream and  
296 downstream chemistry, and upstream and within-slump chemistry. We used this approach to separately  
297 assess the effects of slumping downstream of slump systems, and to compare the composition of slump  
298 runoff to nearby, pristine environments. For each analysis, we included slump location (see Table 1) as a  
299 random effect, and considered models that either nested Julian date within the random effect of slump  
300 location, or allowed Julian date to occur as a fixed effect. The best model was chosen using AIC, and  
301 best-fit models were refit with a variance structure to ensure that model assumptions were met. The  
302 variance structures varIdent (for within-slump site and slump location) and varFixed (for Julian date)  
303 were used together (using varComb) and in isolation for this purpose (Zuur et al., 2009). AIC values for



304 the weighted and un-weighted models were again compared to choose a final model of best fit for each  
305 analysis.

306 We used the high-frequency data from slump FM3 to assess how environmental conditions  
307 (rainfall, temperature, solar radiation) and TSS affect DOC delivery to slump-affected systems. To do  
308 this, we conducted multiple linear regressions, using AIC values to determine models of best fit  
309 (Burnham and Anderson, 2002). To enable a specific assessment of environmental controls on  
310 downstream DOC flux, upstream DOC flux was separated out into a distinct regression analysis, because  
311 upstream DOC flux was strongly correlated with flux downstream, and therefore overwhelmed all  
312 environmental variables in the downstream model. Models were tested for serial correlation using the  
313 auto-correlation function (ACF), and models with variance inflation factors greater than 10 or significant  
314 Durbin Watson test results (indicative of correlated variables; Durbin & Watson, 1950; Hair et al., 1995)  
315 were discarded. Residuals were examined to ensure the model was a good fit for the data (Zuur et al.,  
316 2009). We considered both time-of-sampling (0 h) and past (48, 72, and 120 h) environmental conditions  
317 in our analyses. Because cumulative values for environmental variables (i.e. accumulated rainfall in the  
318 previous 48, 72 and 120 h) showed a strong positive correlation to one another, we used temporally  
319 shifted data (i.e. rainfall 48, 72 and 120 h prior to the DOC flux measurement) in the final model. Similar  
320 models were also constructed to examine the effects of environmental drivers on DOC concentration.  
321 Finally, differences in paired upstream-downstream measures of DOC flux and concentration at slump  
322 FM3 were assessed using a Wilcoxon Signed Rank Test, a non-parametric analog to the paired-t test.

323

324

325 4 Results

326 4.1 *DOC concentration across slump sites*

327 On the Peel Plateau, DOC concentrations consistently declined downstream of slumps, when  
328 compared to paired, upstream locations ( $p < 0.001$ ; Fig. 2; Table 2). Although this effect was modest



329 (typically less than 20%; Fig. 2), it was consistent across all slump sites. In contrast, comparisons of  
330 upstream and within-slump sites showed no consistent trend in DOC concentration, when evaluated  
331 across all slump locations ( $p=0.153$ ; Fig. 2; Table 2). Instead, the effects of slumping on the DOC  
332 concentration of slump runoff appeared to vary by site. At the largest, most well-developed slump  
333 complexes (FM4, FM2, and FM3), where debris tongues are extensive and thaw extends well into the  
334 deepest layer of Pleistocene-aged glacial materials, DOC concentrations tended to be lower in slump  
335 runoff than at the paired upstream sites (Fig. 2). **At more modestly-sized slump sites (HB, HC, and HD),**  
336 **where the modern and relict Holocene active layers form a greater proportion of the actively thawing**  
337 **headwall, within-slump DOC concentrations tended to be higher than values upstream (Fig. 2).** Within  
338 each site, DOC concentrations were relatively consistent across the 2-3 sampling periods. However,  
339 there was significant variation in DOC concentration between slump locations (i.e., across the Peel  
340 Plateau landscape; Fig. 2).

341

#### 342 ***4.2 Bulk chemistry of pristine waters and slump runoff***

343 To better understand how the input of slump runoff affects downstream DOC, we examined  
344 concentrations of conservative ions, conductivity and TSS as ‘tracers’ of slump activity, because these  
345 constituents have previously been shown to be significantly affected by slumping in this region (Kokelj et  
346 al., 2005, 2013; Malone et al., 2013; Thompson et al., 2008). Major ion ( $\text{Ca}^{2+}$ ,  $\text{Mg}^{2+}$ ,  $\text{Na}^+$ ) concentrations  
347 in slump runoff were considerably greater than in pristine streams (a 2.7 to 11.7-fold increase; Fig. 3b-d;  
348 Table 2). These patterns were similar, though muted, at slump-affected downstream sites, where major  
349 ion concentrations were 1.5 to 3.5-fold greater than at pristine sites (Fig. 3b-d; Table 2). Average  
350 conductivity also increased significantly as a result of slumping ( $p < 0.001$ ; Table 2): within-slump sites  
351 had conductivity values that were 9.2-fold greater than upstream sites, while downstream values were  
352 2.6 times greater than those upstream (Fig. 3e). Finally, TSS was also significantly elevated at slump-  
353 affected sites ( $p < 0.001$ ; Table 2) with levels being more than two orders of magnitude greater within



354 slumps when compared to upstream, and more than one order of magnitude greater downstream,  
355 when compared to upstream sites (Fig. 3a).

356

#### 357 *4.3 Spectral and isotopic characteristics*

358 SUVA<sub>254</sub>, which is positively correlated with DOM aromaticity (Weishaar and Aiken, 2003), was  
359 significantly lower within slumps, and downstream of slumps, than in upstream, pristine, environments  
360 ( $p < 0.001$ ; Fig. 4; Table 2). Average within-slump SUVA<sub>254</sub> was less than half of that observed for pristine  
361 waters (Fig. 4), while downstream values declined by approximately 20%. In accordance with the  
362 SUVA<sub>254</sub> results,  $S_{275-295}$ ,  $S_{350-400}$ , and  $S_R$  were all significantly greater within slumps when compared to  
363 upstream sites ( $p < 0.001$ ; Fig. 4; Table 2), indicating lower DOM molecular weight within slumps (Helms  
364 et al., 2008). Differences in slope parameters between upstream and downstream locations were muted  
365 relative to the within-slump: upstream comparisons (Fig. 4), with  $S_{275-295}$  ( $p = 0.011$ ) and  $S_R$  ( $p < 0.001$ )  
366 increasing significantly, but more modestly, downstream of slumps, and  $S_{350-400}$  declining slightly  
367 ( $p = 0.001$ ; Fig. 4; Table 2).

368 Upstream  $\delta^{18}O$  averaged  $-20.1\text{‰} \pm 0.12$ , which corresponds to a modern  $\delta^{18}O$  signature for this  
369 region (Lacelle et al., 2013; Fig. 5). Within-slump  $\delta^{18}O$  was discernibly depleted when compared to  
370 upstream locations, with average values of  $-22.7\text{‰} \pm 0.72$ , which falls between previously-identified  
371 regional endmembers for Pleistocene-aged ground ice ( $18,100 \pm 60$  <sup>14</sup>Cyr BP) and the modern active  
372 layer (Lacelle et al., 2013; Fig. 5). Within-slump  $\delta^{18}O$  was also much more variable between RTS features  
373 than upstream and downstream  $\delta^{18}O$  values. Similar to upstream sites, downstream  $\delta^{18}O$  clustered near  
374 the modern active layer  $\delta^{18}O$  endmember, but with a small depletion that was consistent with a  
375 contribution from slump inflow ( $-20.7\text{‰} \pm 0.21$ ).

376 To further investigate the effect of water source on DOM composition, we examined the  
377 relationship between SUVA<sub>254</sub> and  $\delta^{18}O$ . More depleted samples taken from within-slump sites had  
378 clearly depressed SUVA<sub>254</sub> values when compared to samples with more enriched  $\delta^{18}O$  (Fig. 5). Of the



379 large, most well-developed slumps that were identified in Section 4.1, two (FM2 and FM3), in addition  
380 to site HB, had  $\delta^{18}\text{O}$  values that were more depleted than the Holocene-aged icy diamicton values  
381 reported in Lacelle et al. (2013), suggesting some contribution of runoff from older, Pleistocene-aged  
382 permafrost (Fig. 5). It is likely that the  $\delta^{18}\text{O}$  signal at the relatively stable mega-slump site (FM4) was  
383 somewhat diluted by the 7.2 mm of rainfall that fell in the 48 hours preceding our sample. Although  
384 sites FM3 and SD received 12.4 and 3.5 mm of rain, respectively, in the 48 hours prior to sampling, these  
385 are both much more active slump sites, and thus less prone to dilution of the slump outwash signature.  
386 There was no significant rainfall immediately preceding sampling at any other sites.

387 The radiocarbon signature of DOC from upstream and within-slump locations at sites FM4, FM2,  
388 FM3, and SD largely mirrors the  $\delta^{18}\text{O}$  results. DOC from sites upstream of slump disturbances was  
389 approximately modern in origin (ranging from  $217 \pm 24$   $^{14}\text{C}$  yr BP to modern in age; Table 3). In contrast,  
390 within-slump waters from site FM2 and FM3 were early Holocene-aged ( $9592 \pm 64$ , and  $8167 \pm 39$   $^{14}\text{C}$  yr  
391 BP, respectively; Table 3). Slump runoff from site SD was older than at upstream sites, but younger than  
392 for the larger slumps, described above ( $1157 \pm 23$   $^{14}\text{C}$  yr BP; Table 3).

393

#### 394 **4.4 Patterns and environmental drivers of DOC flux**

395 Similar to our findings for the distributed sampling scheme, downstream DOC concentration was  
396 consistently lower than concentrations upstream, across the 19 paired measurements taken at the  
397 intensively studied slump site (slump FM3;  $p < 0.001$ ,  $N=19$ ,  $W=0$ ; Wilcoxon Signed Rank Test). To explore  
398 environmental drivers of DOC movement within this landscape, however, we focus on DOC flux (as  $\text{mg s}^{-1}$ )  
399  $^1$ ), which allows a direct assessment of slump-mediated DOC addition to this system. Downstream DOC  
400 flux ( $\text{mg s}^{-1}$ ) tended to be slightly greater than upstream flux on most, but not all, sampling occasions  
401 (Fig. 6). As a result, paired comparisons indicate no statistical difference between upstream and  
402 downstream DOC flux at this site (Wilcoxon signed rank test;  $p=0.096$ ,  $N=19$ ,  $W=53$ ). Because upstream  
403 and downstream DOC flux were strongly correlated to one another ( $r^2 = 0.94$ ;  $p < 0.0001$ ), our



404 downstream model was run without upstream DOC flux as a predictor variable. The best-fit multiple  
405 linear regression model for downstream DOC flux ( $r^2 = 0.84$ ;  $p < 0.01$ ) retained seven variables, of which  
406 two were significant (Table 4). Of these, air temperature (72h prior to sampling) showed a negative  
407 relationship with downstream DOC flux and rainfall (0h; time of sampling) showed a strong positive  
408 relationship (Table 4). The best-fit model for upstream DOC flux ( $r^2 = 0.87$ ;  $p < 0.001$ ) also retained seven  
409 variables, of which four were significant ( $p < 0.05$ ; Table 4). Similar to the downstream analysis, air  
410 temperature (0h, 72h) had a negative relationship, and time-of-sampling (0h) rainfall had a strong  
411 positive relationship, with DOC flux (Table 4). However, 120h rainfall showed a negative relationship  
412 with DOC flux in this model. Regressions exploring controls on downstream DOC flux relative to  
413 upstream flux (i.e., as a ratio, or the difference between the two values) were not significant. Models  
414 exploring controls on upstream and downstream DOC concentration were also relatively similar to one  
415 another, showing strong, positive relationships between DOC concentration and air temperature, and  
416 more modest negative relationships between DOC concentration and net radiation (Table 4).

417

418

## 419 5. Discussion

### 420 5.1 Retrogressive thaw slumps and carbon delivery to streams of the Peel Plateau

421 In Eastern Siberia (Drake et al., 2015; Mann et al., 2015; Vonk et al., 2013b), Alaska (Balcarczyk  
422 et al., 2009; Abbott et al., 2014), and the Canadian High Arctic (Melville Island; Woods et al.,  
423 2011), permafrost slumping has been associated with significant increases in DOC mobilization to  
424 streams. Our data show that this was not the case on the Peel Plateau, where the landscape-induced  
425 variation in DOC concentration among pristine stream sites was much greater than the change in stream  
426 water DOC as a result of slumping. Across all of our study sites, DOC concentrations consistently  
427 decreased downstream of slumps when compared to upstream locations. In contrast, comparisons of  
428 channelized slump runoff (our within-slump sites) and paired un-affected sites showed no consistent



429 DOC trend. Instead, DOC concentrations in slump runoff were either greater than, or less than, their  
430 comparison upstream locations, in a manner that differed depending on slump morphological  
431 characteristics such as slump size and headwall height (*Fig. 1; see further discussion in Section 5.3*). The  
432 moderate effect of slumping on DOC concentration occurred despite the significant influence of these  
433 disturbances on the delivery of many biogeochemical constituents to recipient streams. For example,  
434 conductivity was approximately one order of magnitude greater, and TSS two orders of magnitude  
435 greater, in slump-derived runoff than at upstream, un-affected sites.

436         Decreasing DOC concentrations downstream of slumps, despite increasing concentrations of  
437 indicators of slump activity (major ions, TSS) could have several, potentially co-occurring causes. In some  
438 locations, decreases may be partially caused by low DOC concentrations in slump outflow (a dilution  
439 effect; see slumps FM2, FM3, and FM4; Fig. 2). However, field evidence suggests that DOC sorption to  
440 suspended inorganic sediments could also play a role in regulating DOC dynamics in slump-affected  
441 systems on the Peel Plateau. At multiple sites (HB, HC, and HD), DOC concentrations declined  
442 downstream of slumps despite a modest elevation in DOC concentration in slump drainage waters (Fig.  
443 2). Thermokarst contributes significant amounts of glacial sediment to fluvial systems on the Peel  
444 Plateau (Kokelj et al., 2013), and this material is fine-grained (e.g., sediments from the FM3 headwall  
445 have been classified as silty clay; Lacelle et al., 2013). DOC sorption can occur in seconds to minutes in  
446 freshwater systems (Qualls and Haines, 1992), with fine-grained materials being particularly conducive  
447 to these processes (Kothawala et al., 2009). Data from site FM3, where we have upstream and  
448 downstream discharge data coupled with DOC and TSS concentrations at upstream, downstream, and  
449 within-slump locations on two separate dates, allows us to assess possible DOC sorption at this site. On  
450 these dates, DOC flux declines downstream of the slump (i.e.,  $\text{flux}_{\text{DOCdown}} < \text{flux}_{\text{DOCup}}$ ), despite a clear and  
451 measurable efflux of DOC from within the slump (calculated as  $[\text{DOC}]_{\text{within}} \bullet (\text{discharge}_{\text{down}} - \text{discharge}_{\text{up}})$ ;  
452 Fig. 7). This same calculation using TSS as a conservative tracer of slump activity shows the calculated  
453 within-slump flux of TSS (as  $[\text{TSS}]_{\text{within}} \bullet (\text{discharge}_{\text{down}} - \text{discharge}_{\text{up}})$ ) to be almost identical to the



454 difference in TSS flux between downstream and upstream locations (as  $\text{flux}_{\text{TSSdown}} - \text{flux}_{\text{TSSup}}$ ; Fig. 7). Thus,  
455 it is likely that relatively rapid processes such as sorption are affecting DOC dynamics downstream of  
456 slumps on the Peel Plateau.

457       The decrease in DOC concentration downstream of Peel Plateau slumps is similar to, but more  
458 muted than results for lakes in this region, where following slump stabilization, lakes are characterized  
459 by increases in conductivity, clear decreases in DOC concentration, and a strong negative correlation  
460 between these two parameters. The greater magnitude of effect for lakes in this region is likely caused  
461 by substantial particle settling in lentic environments, which enables DOC scavenging with the inorganic  
462 sediment inputs of thermokarst (Kokelj et al., 2005). Although decreasing DOC with RTS activity on the  
463 Peel Plateau contrasts with work to-date in other regions (e.g., Abbott et al., 2014; Vonk et al., 2013a),  
464 ice-marginal glaciated landscapes intensely affected by RTS are common throughout the western  
465 Canadian Arctic, and many other Arctic regions (Kokelj et al., 2017b). In general, this terrain type is  
466 typically characterized by thick, mineral-rich but carbon-poor tills, which with their high ice contents are  
467 predisposed to climate-driven thaw slumping and release of glacial sediments. Thus, it seems likely  
468 that the processes we observe are not limited to the Peel Plateau: research to quantify DOC  
469 ‘sequestration’ via sorption processes seems warranted across regions where thermokarst intensifies  
470 the transport of mineral-rich sediments to downslope aquatic systems.

471

## 472 5.2 The effect of retrogressive thaw slumps on DOM composition

473       Despite the fact that DOC concentrations did not increase in RTS-affected streams,  $\text{SUVA}_{254}$  and  
474 absorbance metrics clearly indicate that slump-derived DOM on the Peel Plateau is compositionally  
475 different than DOM from upstream locations. Upstream waters had significantly higher  $\text{SUVA}_{254}$  values  
476 compared to downstream and within-slump sites (Table 2, Fig. 4). Similarly, while the average  $S_R$  of Peel  
477 Plateau upstream waters ( $0.74 \pm 0.005$ ) was within the range of  $S_R$  typically associated with fresh,  
478 terrestrial DOM ( $\sim 0.70$ ; Helms et al., 2008), values were significantly greater within-slump ( $0.92 \pm 0.015$ )



479 and downstream ( $0.89 \pm 0.009$ ) (Table 2, Fig. 4), indicating decreasing DOM molecular weight as a result  
480 of RTS activity. High  $SUVA_{254}$  values accompanied by low  $S_R$  at upstream sites suggest that water flow in  
481 undisturbed catchments is restricted to shallow, organic-rich flowpaths through the active layer, with  
482 permafrost inhibiting water contributions from deeper, groundwater or mineral-associated sources  
483 (Balcarczyk et al., 2009; MacLean et al., 1999; Mann et al., 2012; O'Donnell et al., 2010). In contrast,  
484 within-slump and downstream measurements indicate a clear transition in DOM source.

485         The comparatively low  $SUVA_{254}$ , and high  $S_R$  values for downstream and within-slump sites  
486 indicate that permafrost-derived carbon on the Peel Plateau is similar in its composition to permafrost  
487 carbon from other regions. For example,  $SUVA_{254}$  values were low in waters draining active thaw slumps  
488 when compared to stabilized and undisturbed sites on the North Slope of Alaska (Abbott et al., 2014),  
489 while in Siberia,  $^{14}C$ -depleted DOM from small tributary streams affected by thermokarst had lower  
490  $SUVA_{254}$  values compared to younger DOM from the Kolyma River mainstem (Mann et al., 2015; Neff et  
491 al., 2006). Although  $SUVA_{254}$  values for waters draining Peel Plateau thaw slumps are slightly lower than  
492 those reported for Siberian Yedoma disturbances (Mann et al., 2015), the overall similarity of  
493 permafrost-derived DOM composition across these various regions is striking, given the regional  
494 differences in permafrost origin and depositional history. For example, while the DOM released by  
495 permafrost thaw on the Peel Plateau is till-associated, and early-Holocene in mean age, east Siberian  
496 Yedoma is composed of loess-derived Pleistocene deposits that sequestered carbon in association with  
497 synengetic aggradation of permafrost. This suggests that common processes may enable the organic  
498 matter contained in permafrost soils to become compositionally similar across diverse Arctic regions.  
499 Such compositional similarity also indicates that permafrost-origin DOM from the Peel Plateau – similar  
500 to that from other regions (Abbott et al., 2014; Drake et al., 2015) – may be readily degraded by  
501 bacteria, despite the divergent origin of this carbon.

502



503 *5.3 The effect of slump morphometry on runoff water biogeochemistry*

504  $\delta^{18}\text{O}$  and  $\text{DO}^{14}\text{C}$  data provide further evidence that intense slumping enables novel sources of  
505 water and solutes to be transported to fluvial systems on the Peel Plateau. For most of the RTS features  
506 that we studied, the  $\delta^{18}\text{O}$  signature of within-slump waters ranged from those similar to the 'icy  
507 diamicton' that overlies the early Holocene thaw unconformity, to those for underlying Pleistocene-aged  
508 ground ice (Lacelle et al., 2013; Fig. 5). Similarly,  $\text{DO}^{14}\text{C}$  from a subset of sites indicates slump-derived  
509 DOC is early Holocene-aged for all but the shallowest slump surveyed. This suggests that our slump  
510 outflow samples were likely comprised of a mixture of Pleistocene-, Holocene-, and modern-sourced  
511 water (see Fig. 1c-e), but that **the contribution of these end-members varied across slumps.**

512 The between-site variation in  $\delta^{18}\text{O}$  signature (Fig. 5) and relative DOC concentration (Fig. 2b) of  
513 slump runoff waters appears to be related to differences in slump morphometry (size, headwall height,  
514 and the length and area of the debris tongue; see Table 1 and Fig. 1c-e) across sites. The well-developed,  
515 larger slump complexes (FM4, FM2 and FM3) were more likely to have  $\delta^{18}\text{O}$  signatures that lie between  
516 end-member values for icy diamicton and Pleistocene-aged ground ice (Fig. 5; although note that dry  
517 and stabilized FM4 differs somewhat from this trend). These well-developed slumps also stood out as  
518 displaying within-slump DOC concentrations that were lower than at upstream comparison sites (Fig.  
519 2b). The headwall ~~exposure~~ at these largest slumps exposes Pleistocene-aged permafrost to several  
520 metres depth (see Fig. 1c), while the evacuation of scar zone materials have produced extensive debris  
521 tongues up to several kilometers long (Table 1, Figs. 1b, S1e and S1g). This significant exposure of  
522 mineral-rich, Pleistocene-aged glacial till contributes solutes from low-carbon mineral soils to runoff,  
523 while entraining fine-grained sediments which provide mineral surface area for possible DOC  
524 adsorption. Adsorption may be further enhanced as slump and stream runoff continue to entrain  
525 sediments as flows incise the lengthy debris tongue deposits. In contrast, slumps with slightly shallower  
526 headwalls (HA, HB, HC, HD; see Fig. 1d), and less well-developed debris tongues (Table 1), appear to  
527 elicit a slightly different response than the largest slumps discussed above. At these mid-sized sites,



528 within-slump DOC concentrations were typically higher than those found at upstream comparison sites  
529 (Fig. 2b), which may reflect the greater relative inputs from thawing of the Holocene-aged active layer,  
530 and decreased interaction with debris tongue deposits at these smaller disturbances. Similarly, runoff  
531  $\delta^{18}\text{O}$  tends to lie between Holocene and modern end-member values at these sites (though note the  
532 more depleted value for HB; Fig. 5), indicating a lower relative contribution of Pleistocene-aged ground  
533 ice.

534 Finally, the youngest and shallowest slump surveyed (SD), exposes only near-surface permafrost  
535 soils for leaching and geochemical transport (Figs. 1e and S1; Table 1), and not the underlying mineral  
536 and ice-rich glacial substrates. Accordingly, the effects of slumping on stream chemistry, optical  
537 parameters, and isotopes appear muted at SD when compared to the larger slumps discussed above.  
538 These morphometry-related shifts in downstream effect suggest that we should expect non-linearity in  
539 the biogeochemical response as slump features develop over time, particularly if slumping continues to  
540 intensify with future warming on the Peel Plateau (e.g., Kokelj et al., 2017b). Long-term monitoring, and  
541 the incorporation of non-linearity into models predicting future change, are clearly warranted for the  
542 Peel Plateau and elsewhere in the Arctic.

543

#### 544 *5.4 Environmental controls on DOC flux and concentration*

545 Air temperature and rainfall exerted the strongest control on DOC flux at our intensively studied  
546 site (slump FM3; Fig. 6; Table 4). Upstream of the slump, rainfall was positively correlated, and air  
547 temperature negatively correlated, with DOC flux. However, precipitation events are negatively related  
548 to temperature at this site (Fig. 6), suggesting that at the single-season scale of our investigation,  
549 precipitation served as the primary environmental control on DOC flux. DOC concentration was  
550 relatively constant with discharge at the upstream site ( $r=-0.342$ ,  $p=0.151$ ), indicating that precipitation  
551 controls DOC flux largely as a result of changes in water flow at this site, and that DOC was not **source**  
552 **limited** over the time scale of our investigation. **DOC concentration was positively related to**



553 temperature, however (Table 4), suggesting that biological activity is an important regulator of within-  
554 soil DOC production (c.f. Pumpanen et al., 2014). These upstream-of-slump results are consistent with  
555 work from other undisturbed permafrost and boreal regions, where precipitation and catchment runoff  
556 have been shown to control DOC flux in streams (Prokushkin et al., 2005; Pumpanen et al., 2014), and  
557 increasing temperature has been shown to increase DOC production in soils (Christ and David, 1996;  
558 Neff and Hooper, 2002; Prokushkin et al., 2005; Yanagihara et al., 2000). They are also consistent with  
559 the concept that the impermeable permafrost barrier forces precipitation to travel through the shallow  
560 active layer, where high hydraulic conductivity leads to rapid transport of carbon into fluvial systems,  
561 and little degradation in soils (O'Donnell et al., 2010; Striegl et al., 2005).

562 Slumping did not significantly modify downstream DOC flux at the intensively studied slump site,  
563 when compared to DOC flux upstream of slump FM3 (Fig. 6; Section 4.4). Although concentration  
564 consistently declined downstream at this site (Sections 4.1 and 4.4), downstream flux was either slightly  
565 higher, or slightly lower, than upstream values, across the multiple measurement points that we  
566 considered. Concordant with this finding, neither the ratio of (downstream: upstream) or difference  
567 between (downstream – upstream) upstream and downstream DOC flux could be explained by any of  
568 our environmental variables, while downstream flux showed an almost identical relationship with  
569 environmental controls as those upstream (Table 4). The lack of clear environmental control on relative  
570 downstream: upstream DOC flux occurred despite the fact that precipitation has been shown to be a  
571 strong driver of ablation and sediment movement from slump features on the Peel Plateau, at time  
572 scales similar to those used for this work (Kokelj et al., 2015).

573 Considering the Peel Plateau landscape as a whole, it appears that precipitation serves as a  
574 primary, positive control on DOC flux. Thus, this study adds DOC production to the list of changes – such  
575 as increasing slump activity and sediment mobilization – that can be expected with the increases in  
576 precipitation that are underway in this region, and are expected throughout the Arctic (Kokelj et al.,  
577 2015; Walsh et al., 2011). However, it appears that slumping does not over-ride the landscape-scale



578 control on DOC flux in this system – at least at the scale of this single-season – perhaps because  
579 processes like DOC sorption mask the influx of slump-derived DOC (Fig. 6). This result clearly highlights  
580 the complexity of the interaction between changing climatic parameters and DOC dynamics on the Peel  
581 Plateau, where slump features of increasing size incorporate thawing till, glaciolacustrine, glaciofluvial,  
582 and organic deposits; additionally drain contemporary active layers across a shrub-tundra to spruce  
583 forest upland gradient; and where DOC dynamics are variably affected by both water and carbon  
584 generation across these landform types, and biogeochemical interactions such as mineral adsorption in  
585 recipient systems. It also underscores the need for future work to tease apart the interactions between  
586 changing climatic parameters, slump development, and resultant biogeochemical effects; both on the  
587 Peel Plateau and across the Arctic, where environmental controls on slump activity and thus  
588 downstream biogeochemistry can be expected to show marked regional variation (see for example,  
589 work from Eureka Sound; Grom & Pollard 2008).

590

591 *5.5 Study implications and future research directions: dissolved carbon mobilization across diverse*  
592 *permafrost landscapes*

593 Carbon dynamics in Arctic aquatic systems are influenced by numerous factors, including  
594 geology, Quaternary and glacial history, soil composition, vegetation, active layer dynamics and the  
595 nature and intensity of thermokarst. As a result, the effect of permafrost thaw on DOC concentration  
596 and flux should – at a fundamental level – vary across broad, regional scales. This study demonstrates  
597 that we can expect large inter-regional variations in DOC transport to streams in response to permafrost  
598 degradation, and that results from multiple regions are needed to understand change across the Arctic  
599 as whole. The declines in DOC concentration downstream of slumps on the Peel Plateau differ strikingly  
600 from what has been found in eastern Siberia and regions of Alaska, for example, where thermokarst  
601 releases substantial quantities of DOC (e.g., Spencer et al. 2015), and significantly increases DOC  
602 concentrations in downstream systems (Abbott et al. 2015). Modelling efforts that incorporate



603 information concerning the geology and Quaternary history of landscapes that are being thawed, the  
604 physical and geochemical composition of permafrost soils, and the nature and intensity of the  
605 thermokarst processes within landscapes would clearly enable more accurate predictions of how carbon  
606 delivery from land to water will respond to climate change on a pan-Arctic scale.

607 At finer scales, however, this work underlines the variability of thermokarst effects within  
608 regions, and the local-scale control on this variability. On the Peel Plateau, for example, between-site  
609 difference in the biogeochemical effect of thermokarst corresponds to variation in soil stratigraphy (i.e.,  
610 the relative depth of the paleo-active layer) and ever-evolving slump morphometry. **Although striking**  
611 **within-region variability in the biogeochemical effects of thermokarst has been seen elsewhere (e.g.,**  
612 **Watanabe et al., 2011), it occurs a result of very different landscape-level drivers. This landscape-**  
613 **specificity also extends to the non-linearity of the biogeochemical response as slump features develop**  
614 **over time.** The changing response of downstream biogeochemistry with slump development is very  
615 different on the Peel Plateau, ~~for example,~~ than in other regions (e.g., Abbot et al. 2015), while non-  
616 linearity can also be expected to extend to different types of permafrost thaw, such as increasing active  
617 layer thickness (**Kokelj et al. 2002, Vonk et al. 2016**). Only with a tiered approach, where we focus within  
618 regions to understand local controls and changing effects over time, and across regions to document  
619 how predictable, broad-scale variation affects the nature of thermokarst effects, will we be able to truly  
620 understand the future biogeochemical functioning of thermokarst-affected landscapes at the pan-Arctic  
621 scale.

622

623

#### 624 **Acknowledgements**

625 Financial support for this research was provided by Ontario Graduate Scholarship, York University

626 Fieldwork Cost Fund, York University Research Cost Fund, Northern Scientific Training Program, NSERC

627 Discovery and Northern Research Supplement grants to SET, the Campus Alberta Innovates Program,



628 and the Polar Continental Shelf Program. We would like to thank Scott Zolkos for his support as a field  
629 assistant and for the production of Figure 1; S. Tetlichi, D. Neyando, and P. Snowshoe for field sampling  
630 assistance; and the Tetlit Gwich'in (Fort McPherson) Renewable Resources Council. Sarah Shakil and  
631 Scott Zolkos assisted with the collection of samples for  $\text{DO}^{14}\text{C}$ ; Justin Kokoszka performed geospatial  
632 calculations of slump area and debris tongue length.



633 **Literature Cited**

- 634 Abbott, B. W., Larouche, J. R., Jones, J. B., Bowden, W. B., and Balsler, A. W.: Elevated dissolved organic  
635 carbon biodegradability from thawing and collapsing permafrost, *J. Geophys. Res.*, 119, 2049–2063,  
636 doi:10.1002/2014JG002678, 2014.
- 637 Abbott, B. W., Jones, J. B., Godsey, S. E., Larouche, J. R., and Bowden, W. B.: Patterns and persistence of  
638 hydrologic carbon and nutrient export from collapsing upland permafrost, *Biogeosciences*, 12, 3725–  
639 3740, doi:10.5194/bg-12-3725-2015, 2015.
- 640 Balcarczyk, K. L., Jones, J. B., Jaffé, R., and Maie, N.: Stream dissolved organic matter bioavailability and  
641 composition in watersheds underlain with discontinuous permafrost, *Biogeochemistry*, 94, 255–270,  
642 doi:10.1007/s10533-009-9324-x, 2009.
- 643 Battin, T. J., Kaplan, L. A., Findlay, S., Hopkinson, C. S., Marti, E., Packman, A. I., Newbold, J. D., and  
644 Sabater, F.: Biophysical controls on organic carbon fluxes in fluvial networks, *Nat. Geosci.*, 1, 95–100,  
645 doi:10.1038/ngeo101, 2008.
- 646 Burn, C. R. and Kokelj, S. V.: The environment and permafrost of the Mackenzie Delta area, *Permafr.*  
647 *Periglac. Process.*, 20, 83–105, doi:10.1002/ppp.655, 2009.
- 648 Burnham, K. P. and Anderson, D. R.: *Model Selection and Multi- Model Inference: A Practical*  
649 *Information-Theoretic Approach*, Springer, New York., 2002.
- 650 Catto, N. R.: Richardson Mountains, Yukon-Northwest Territories: The northern portal of the postulated  
651 “Ice-Free Corridor,” *Quat. Int.*, 32, 3–19, doi:10.1016/1040-6182(95)00062-3, 1996.
- 652 Chin, K. S., Lento, J., Culp, J. M., Lacelle, D., and Kokelj, S. V.: Permafrost thaw and intense thermokarst  
653 activity decreases abundance of stream benthic macroinvertebrates, *Glob. Chang. Biol.*, 22, 2715–2728,  
654 doi:10.1111/gcb.13225, 2016.
- 655 Christ, M. J. and David, M. B.: Temperature and moisture effects on the production of dissolved organic  
656 carbon in a Spodosol, *Soil Biol. Biochem.*, 28, 1191–1199, doi:10.1016/0038-0717(96)00120-4, 1996.
- 657 Curtin, J.: *lmSupport: Support for Linear Models*. R package version 2.9.2., 2015.
- 658 Dittmar, T. and Kattner, G.: The biogeochemistry of the river and shelf ecosystem of the Arctic Ocean: a  
659 review, *Mar. Chem.*, 83, 103–120, doi:10.1016/S0304-4203(03)00105-1, 2003.
- 660 Drake, T. W., Wickland, K. P., Spencer, R. G. M., McKnight, D. M., and Striegl, R. G.: Ancient low-  
661 molecular-weight organic acids in permafrost fuel rapid carbon dioxide production upon thaw, *Proc.*  
662 *Natl. Acad. Sci.*, 112, 13946–13951, doi:10.1073/pnas.1511705112, 2015.
- 663 Duk-Rodkin, A. and Hughes, O. L.: Surficial geology, Fort McPherson-Bell River. Yukon-Northwest  
664 Territories. Geological Survey of Canada, Map 1745A, scale 1:250 000, Geological Survey of Canada, Map  
665 1745A, scale 1:250 000., 1992.
- 666 Durbin, J. and Watson, G. S.: Testing for serial correlation in least squares regression I, *Biometrika*, 37,  
667 409–428, 1950.
- 668 Environment Canada: Canadian Climate Normals 1981-2010 Station Data, Fort McPherson, 2015.
- 669 Fox, J. and Weisberg, S.: *An {R} Companion to Applied Regression*, Second Edition. Thousand Oaks CA:



- 670 Sage. <http://socserv.socsci.mcmaster.ca/jfox/Books/Companion.>, 2011.
- 671 Frey, K. E. and McClelland, J. W.: Impacts of permafrost degradation on arctic river biogeochemistry,  
672 *Hydrol. Process.*, 23, 169–182, doi:10.1002/hyp, 2009.
- 673 Fulton, R. J.: *Surficial Materials of Canada*, Natural Resources Canada., 1995.
- 674 Green, S. A. and Blough, N. V.: Optical absorption and fluorescence properties of chromophoric  
675 dissolved organic matter in natural waters, *Limnol. Oceanogr.*, 39, 1903–1916,  
676 doi:10.4319/lo.1994.39.8.1903, 1994.
- 677 Hair, J. F. J., Anderson, R. E., Tatham, R. L., and Black, W. C.: *Multivariate Data Analysis*, 3rd ed.,  
678 Macmillan, New York., 1995.
- 679 Hedges, J. I., Keil, R. G., and Benner, R.: What happens to terrestrial organic matter in the ocean?, *Org.*  
680 *Geochem.*, 27, 195–212, 1997.
- 681 Helms, J. R., Stubbins, A., Ritchie, J. D., Minor, E. C., Kieber, D. J., and Mopper, K.: Absorption spectral  
682 slopes and slope ratios as indicators of molecular weight, source, and photobleaching of chromophoric  
683 dissolved organic matter, *Limnol. Oceanogr.*, 53, 955–969, doi:10.4319/lo.2008.53.3.0955, 2008.
- 684 Holmes, R. M., McClelland, J. W., Peterson, B. J., Tank, S. E., Bulygina, E., Eglinton, T. I., Gordeev, V. V.,  
685 Gurtovaya, T. Y., Raymond, P. A., Repeta, D. J., Staples, R., Striegl, R. G., Zhulidov, A. V., and Zimov, S. A.:  
686 Seasonal and annual fluxes of nutrients and organic matter from large rivers to the Arctic Ocean and  
687 surrounding seas, *Estuaries and Coasts*, 35, 369–382, doi:10.1007/s12237-011-9386-6, 2012.
- 688 Hugelius, G., Strauss, J., Zubrzycki, S., Harden, J. W., Schuur, E. A. G., Ping, C. L., Schirmer, L., Grosse,  
689 G., Michaelson, G. J., Koven, C. D., O'Donnell, J. A., Elberling, B., Mishra, U., Camill, P., Yu, Z., Palmtag, J.,  
690 and Kuhry, P.: Estimated stocks of circumpolar permafrost carbon with quantified uncertainty ranges  
691 and identified data gaps, *Biogeosciences*, 11, 6573–6593, doi:10.5194/bg-11-6573-2014, 2014.
- 692 IPCC: *Climate Change 2014: Synthesis Report. Contribution of Working Groups I, II and III to the Fifth*  
693 *Assessment Report of the Intergovernmental Panel on Climate Change [Core Writing Team, R.K.*  
694 *Pachauri and L.A. Meyer (eds.)]. IPCC, Geneva, Switzerland, 151 pp, Geneva, Switzerland., 2014.*
- 695 Kaiser, K. and Guggenberger, G.: The role of DOM sorption to mineral surfaces in the preservation of  
696 organic matter in soils, *Org. Geochem.*, 31, 711–725, doi:10.1016/S0146-6380(00)00046-2, 2000.
- 697 Khvorostyanov, D. V., Krinner, G., Ciais, P., Heimann, M., and Zimov, S. A.: Vulnerability of permafrost  
698 carbon to global warming. Part I: Model description and role of heat generated by organic matter  
699 decomposition, *Tellus, Ser. B Chem. Phys. Meteorol.*, 60 B, 250–264, doi:10.1111/j.1600-  
700 0889.2007.00333.x, 2008a.
- 701 Khvorostyanov, D. V., Ciais, P., Krinner, G., Zimov, S. A., Corradi, C., and Guggenberger, G.: Vulnerability  
702 of permafrost carbon to global warming. Part II: Sensitivity of permafrost carbon stock to global  
703 warming, *Tellus, Ser. B Chem. Phys. Meteorol.*, 60 B, 265–275, doi:10.1111/j.1600-0889.2007.00336.x,  
704 2008b.
- 705 Kokelj, S. V., Tunnicliffe, J. F., and Lacelle, D.: The Peel Plateau of northwestern Canada : an ice-rich  
706 hummocky moraine landscape in transition, in *Landscapes and Landforms of Western Canada*, edited by  
707 O. Slaymaker, pp. 109–122, Springer International Publishing, Switzerland., 2017a.



- 708 Kokelj, S. V. and Jorgenson, M. T.: Advances in thermokarst research, *Permafr. Periglac. Process.*, 24,  
709 108–119, doi:10.1002/ppp.1779, 2013.
- 710 Kokelj, S. V., Smith, C. A., and Burn, C. R.: Physical and chemical characteristics of the active layer and  
711 permafrost, Herschel Island, western Arctic Coast, Canada, *Permafr. Periglac. Process.*, 13, 171–185,  
712 doi:10.1002/ppp.417, 2002.
- 713 Kokelj, S. V., Jenkins, R. E., Milburn, D., Burn, C. R., and Snow, N.: The influence of thermokarst  
714 disturbance on the water quality of small upland lakes, Mackenzie Delta region, Northwest Territories,  
715 Canada, *Permafr. Periglac. Process.*, 16, 343–353, doi:10.1002/ppp.536, 2005.
- 716 Kokelj, S. V., Lantz, T. C., Kanigan, J. C., Smith, S. L., and Coutts, R.: Origin and polycyclic behaviour of  
717 tundra thaw slumps, Mackenzie Delta region, Northwest Territories, Canada, *Permafr. Periglac. Process.*,  
718 20, 173–184, doi:10.1002/ppp, 2009.
- 719 Kokelj, S. V., Lacelle, D., Lantz, T. C., Tunnicliffe, J., Malone, L., Clark, I. D., and Chin, K. S.: Thawing of  
720 massive ground ice in mega slumps drives increases in stream sediment and solute flux across a range of  
721 watershed scales, *J. Geophys. Res. Earth Surf.*, 118, 681–692, doi:10.1002/jgrf.20063, 2013.
- 722 Kokelj, S. V., Tunnicliffe, J., Lacelle, D., Lantz, T. C., Chin, K. S., and Fraser, R.: Increased precipitation  
723 drives mega slump development and destabilization of ice-rich permafrost terrain, northwestern  
724 Canada, *Glob. Planet. Change*, 129, 56–68, doi:10.1016/j.gloplacha.2015.02.008, 2015.
- 725 Kokelj, S. V., Lantz, T. C., Tunnicliffe, J., Segal, R., and Lacelle, D.: Climate-driven thaw of permafrost  
726 preserved glacial landscapes, northwestern Canada, *Geology*, 45, 371–374, doi:10.1130/G38626.1,  
727 2017b.
- 728 Kothawala, D. N., Moore, T. R., and Hendershot, W. H.: Soil properties controlling the adsorption of  
729 dissolved organic carbon to mineral soils, *Soil Sci. Soc. Am. J.*, 73, 1831, doi:10.2136/sssaj2008.0254,  
730 2009.
- 731 Lacelle, D., Bjornson, J., and Lauriol, B.: Climatic and geomorphic factors affecting contemporary (1950-  
732 2004) activity of retrogressive thaw slumps on the Aklavik plateau, Richardson mountains, NWT, Canada,  
733 *Permafr. Periglac. Process.*, 21, 1–15, doi:10.1002/ppp.666, 2010.
- 734 Lacelle, D., Lauriol, B., Zazula, G., Ghaleb, B., Utting, N., and Clark, I. D.: Timing of advance and basal  
735 condition of the Laurentide Ice Sheet during the last glacial maximum in the Richardson Mountains,  
736 NWT, *Quat. Res. (United States)*, 80, 274–283, doi:10.1016/j.yqres.2013.06.001, 2013.
- 737 Lacelle, D., Fontaine, M., Forest, A. P., and Kokelj, S.: High-resolution stable water isotopes as tracers of  
738 thaw unconformities in permafrost: A case study from western Arctic Canada, *Chem. Geol.*, 368, 85–96,  
739 doi:10.1016/j.chemgeo.2014.01.005, 2014.
- 740 Lacelle, D., Brooker, A., Fraser, R. H., and Kokelj, S. V.: Distribution and growth of thaw slumps in the  
741 Richardson Mountains–Peel Plateau region, northwestern Canada, *Geomorphology*, 235, 40–51,  
742 doi:10.1016/j.geomorph.2015.01.024, 2015.
- 743 Lafrenière, M. J. and Lamoureux, S. F.: Thermal perturbation and rainfall runoff have greater impact on  
744 seasonal solute loads than physical disturbance of the active layer, *Permafr. Periglac. Process.*, 24, 241–  
745 251, doi:10.1002/ppp.1784, 2013.
- 746 Lang, S. Q., McIntyre, C. P., Bernasconi, S. M., Früh-Green, G. L., Voss, B. M., Eglinton, T. I., and Wacker,



- 747 L.: Rapid  $^{14}\text{C}$  analysis of dissolved organic carbon in non-saline waters, *Radiocarbon*, 58, 505–515,  
748 doi:10.1017/RDC.2016.17, 2016.
- 749 Lantuit, H. and Pollard, W. H.: Fifty years of coastal erosion and retrogressive thaw slump activity on  
750 Herschel Island, southern Beaufort Sea, Yukon Territory, Canada, *Geomorphology*, 95, 84–102,  
751 doi:10.1016/j.geomorph.2006.07.040, 2008.
- 752 Lantz, T. C. and Kokelj, S. V.: Increasing rates of retrogressive thaw slump activity in the Mackenzie Delta  
753 region, N.W.T., Canada, *Geophys. Res. Lett.*, 35, 1–5, doi:10.1029/2007GL032433, 2008.
- 754 Lewkowicz, A. G.: Rate of short-term ablation of exposed ground ice, Banks Island, Northwest  
755 Territories, Canada, *J. Glaciol.*, 32, 511–519, 1986.
- 756 Lewkowicz, A. G.: Headwall retreat of ground-ice slumps, Banks Island, Northwest Territories, *Can. J.*  
757 *Earth Sci.*, 24, 1077–1085, doi:10.1139/e87-105, 1987.
- 758 MacLean, R., Oswood, M. W., Irons, J. G., and McDowell, W. H.: The effect of permafrost on stream  
759 biogeochemistry: A case study of two streams in the Alaskan (U.S.A.) taiga, *Biogeochemistry*, 47, 239–  
760 267, doi:10.1007/BF00992909, 1999.
- 761 Malone, L., Lacelle, D., Kokelj, S., and Clark, I. D.: Impacts of hillslope thaw slumps on the geochemistry  
762 of permafrost catchments (Stony Creek watershed, NWT, Canada), *Chem. Geol.*, 356, 38–49,  
763 doi:10.1016/j.chemgeo.2013.07.010, 2013.
- 764 Manley, W. F. and Kaufman, D. S.: *Alaska PaleoGlacier Atlas: Institute of Arctic and Alpine Research*  
765 (INSTAAR), University of Colorado., 2002.
- 766 Mann, P. J., Davydova, A., Zimov, N., Spencer, R. G. M., Davydov, S., Bulygina, E., Zimov, S., and Holmes,  
767 R. M.: Controls on the composition and lability of dissolved organic matter in Siberia's Kolyma River  
768 basin, *J. Geophys. Res. Biogeosciences*, 117, 1–15, doi:10.1029/2011JG001798, 2012.
- 769 Mann, P. J., Eglinton, T. I., McIntyre, C. P., Zimov, N., Davydova, A., Vonk, J. E., Holmes, R. M., and  
770 Spencer, R. G. M.: Utilization of ancient permafrost carbon in headwaters of Arctic fluvial networks, *Nat.*  
771 *Commun.*, 6, doi: 10.1038/ncomms8856, 2015.
- 772 McDowell, W. H.: Kinetics and mechanisms of dissolved organic carbon retention in a headwater stream,  
773 *Biogeochemistry*, 1, 329–352, 1985.
- 774 McGuire, A. D., Anderson, L. G., Christensen, T. R., Dallimore, S., Guo, L., Hayes, D. J., Heimann, M.,  
775 Lorenson, T. D., MacDonald, R. W., and Roulet, N.: Sensitivity of the carbon cycle in the Arctic to climate  
776 change, *Ecol. Monogr.*, 79, 523–555, doi:10.1890/08-2025.1, 2009.
- 777 Murton, J. and French, H.: Cryostructures in permafrost, Tuktoyaktuk coastlands, western arctic Canada,  
778 *Can. J. Earth Sci.*, 31, 737–747, doi:10.1139/e94-067, 1994.
- 779 Murton, J. B., Edwards, M. E., Lozhkin, A. V., Anderson, P. M., Savvinov, G. N., Bakulina, N., Bondarenko,  
780 O. V., Cherepanova, M. V., Danilov, P. P., Boeskorov, V., Goslar, T., Grigoriev, S., Gubin, S. V., Korzun, J. A.,  
781 Lupachev, A. V., Tikhonov, A., Tsygankova, V. I., Vasilieva, G. V., and Zanina, O. G.: Preliminary  
782 paleoenvironmental analysis of permafrost deposits at Batagaika megaslump, Yana Uplands, northeast  
783 Siberia, *Quat. Res.*, 87, 314–330, doi:10.1017/qua.2016.15, 2017.
- 784 Neff, J. C. and Hooper, D. U.: Vegetation and climate controls on potential  $\text{CO}_2$ , DOC and DON



- 785 production in northern latitude soils, *Glob. Chang. Biol.*, 8, 872–884, doi:10.1046/j.1365-  
786 2486.2002.00517.x, 2002.
- 787 Neff, J. C., Finlay, J. C., Zimov, S. A., Davydov, S. P., Carrasco, J. J., Schuur, E. A. G., and Davydova, A. I.:  
788 Seasonal changes in the age and structure of dissolved organic carbon in Siberian rivers and streams,  
789 *Geophys. Res. Lett.*, 33, 1–5, doi:10.1029/2006GL028222, 2006.
- 790 Norris, D. K.: Geology of the northern Yukon and northwestern District of Mackenzie. Geological Survey  
791 of Canada, Map 1581A, scale 1:500 000., 1984.
- 792 O'Donnell, J. A., Aiken, G. R., Kane, E. S., and Jones, J. B.: Source water controls on the character and  
793 origin of dissolved organic matter in streams of the Yukon River basin, Alaska, *J. Geophys. Res.*  
794 *Biogeosciences*, 115, 1–12, doi:10.1029/2009JG001153, 2010.
- 795 Palstra, S. and Meijer, H.: Biogenic carbon fraction of biogas and natural gas fuel mixtures determined  
796 with  $^{14}\text{C}$ , *Radiocarbon*, 56, 7–28, doi:10.2458/56.16514, 2014.
- 797 Pinheiro, J., Bates, D., DebRoy, S., Sarkar, D., and R Core Team: nlme: Linear and nonlinear mixed effects  
798 models. R package version 3.1-120, <http://CRAN.R-project.org/package=nlme>, 2015.
- 799 Poulin, B. A., Ryan, J. N., and Aiken, G. R.: Effects of iron on optical properties of dissolved organic  
800 matter, *Environ. Sci. Technol.*, 48, 10098–10106, doi:10.1021/es502670r, 2014.
- 801 Prokushkin, A. S., Kajimoto, T., Prokushkin, S. G., McDowell, W. H., Abaimov, A. P., and Matsuura, Y.:  
802 Climatic factors influencing fluxes of dissolved organic carbon from the forest floor in a continuous-  
803 permafrost Siberian watershed, *Can. J. For. Res.*, 35, 2130–2140, doi:10.1139/x05-150, 2005.
- 804 Pumpanen, J., A, L., Heli, M., Kolari, P., Ilvesniemi, H., Mammarella, I., Hari, O., Nikinmaa, E., Heinonsalo,  
805 J., Back, J., Ojala, A., Berninger, F., and Vesala, T.: Precipitation and net ecosystem exchange are the  
806 most important drivers of DOC flux in upland boreal catchments, *J. Geophys. Res. Biogeosciences*, 119,  
807 1861–1878, doi:10.1002/2014JG002705, 2014.
- 808 Qualls, R. and Haines, B. L.: Measuring adsorption isotherms using continuous, unsaturated flow through  
809 intact soil cores, *Soil Sci. Soc. Am. J.*, 56, 456–460, doi:10.2136/sssaj1992.03615995005600020019x,  
810 1992.
- 811 R Core Team: R: A Language and Environment for Statistical Computing, R Foundation for Statistical  
812 Computing, Vienna, Austria. <http://www.r-project.org/>, 2015.
- 813 Rampton, V. N.: Quaternary geology of the Tuktoyaktuk coastlands, Northwest Territories, *Geol. Surv.*  
814 *Canada*, 1988.
- 815 Schuur, E., Bockheim, J., Canadell, J. G., Euskirchen, E., Field, C. B., Goryachkin, S. V., Hagemann, S.,  
816 Kuhry, P., Lafleur, P. M., Lee, H., Nelson, M. F. E., Rinke, A., Romanovsky, V. E., Shiklomanov, N.,  
817 Tarnocai, C., Venevsky, S., Vogel, J. G., and Zimov, S. A.: Vulnerability of permafrost carbon to climate  
818 change : Implications for the global carbon cycle, *Bioscience*, 58, 701–714, doi:10.1641/B580807, 2008.
- 819 Schuur, E. A. G., Abbott, B. W., Bowden, W. B., Brovkin, V., Camill, P., Canadell, J. G., Chanton, J. P.,  
820 Chapin, F. S., Christensen, T. R., Ciais, P., Crosby, B. T., Czimczik, C. I., Grosse, G., Harden, J., Hayes, D. J.,  
821 Hugelius, G., Jastrow, J. D., Jones, J. B., Kleinen, T., Koven, C. D., Krinner, G., Kuhry, P., Lawrence, D. M.,  
822 McGuire, A. D., Natali, S. M., O'Donnell, J. A., Ping, C. L., Riley, W. J., Rinke, A., Romanovsky, V. E., Sannel,  
823 A. B. K., Schädel, C., Schaefer, K., Sky, J., Subin, Z. M., Tarnocai, C., Turetsky, M. R., Waldrop, M. P.,



- 824 Walter Anthony, K. M., Wickland, K. P., Wilson, C. J., and Zimov, S. A.: Expert assessment of vulnerability  
825 of permafrost carbon to climate change, *Clim. Change*, 119, 359–374, doi:10.1007/s10584-013-0730-7,  
826 2013.
- 827 Schuur, E. A. G., McGuire, A. D., Grosse, G., Harden, J. W., Hayes, D. J., Hugelius, G., Koven, C. D. and  
828 Kuhry, P.: Climate change and the permafrost carbon feedback, *Nature*, 520, 171–179,  
829 doi:10.1038/nature14338, 2015.
- 830 Segal, R. A., Lantz, T. C., and Kokelj, S. V: Acceleration of thaw slump activity in glaciated landscapes of  
831 the Western Canadian Arctic, *Environ. Res. Lett.*, 11, 34025, doi:10.1088/1748-9326/11/3/034025, 2016.
- 832 Spencer, R. G. M., Mann, P. J., Dittmar, T., Eglinton, T. I., Mcintyre, C., Holmes, R. M., Zimov, N., and  
833 Stubbins, A.: Detecting the signature of permafrost thaw in Arctic rivers, *Geophys. Res. Lett.*, 42,  
834 doi:10.1002/2015GL063498, doi:10.1002/2015GL063498, 2015.
- 835 Striegl, R. G., Aiken, G. R., Dornblaser, M. M., Raymond, P. A., and Wickland, K. P.: A decrease in  
836 discharge-normalized DOC export by the Yukon River during summer through autumn, *Geophys. Res.*  
837 *Lett.*, 32, 1–4, doi:10.1029/2005GL024413, 2005.
- 838 Tank, S. E., Raymond, P. A., Striegl, R. G., McClelland, J. W., Holmes, R. M., Fiske, G. J., and Peterson, B.  
839 J.: A land-to-ocean perspective on the magnitude, source and implication of DIC flux from major Arctic  
840 rivers to the Arctic Ocean, *Global Biogeochem. Cycles*, 26, n/a-n/a, doi:10.1029/2011GB004192, 2012a.
- 841 Tank, S. E., Manizza, M., Holmes, R. M., McClelland, J. W., and Peterson, B. J.: The Processing and impact  
842 of dissolved riverine nitrogen in the Arctic Ocean, *Estuaries and Coasts*, 35, 401–415,  
843 doi:10.1007/s12237-011-9417-3, 2012b.
- 844 Tanski, G., Couture, N., Lantuit, H., Eulenburg, A., and Fritz, M.: Eroding permafrost coasts release low  
845 amounts of dissolved organic carbon (DOC) from ground ice into the nearshore zone of the Arctic Ocean,  
846 *Glob. Biogeochem. Cycles*, 30, 1054–1068, doi:10.1002/2015GB005337, 2016.
- 847 Thompson, M. S., Prowse, T. D., Kokelj, S. V., and Wrona, F. J.: The impact of sediments derived from  
848 thawing permafrost on tundra lake water chemistry: An experimental approach, *Proc. Ninth Int. Conf.*  
849 *Permafr.*, 29, 1763–1768, 2008.
- 850 Vonk, J. E. and Gustafsson, Ö.: Permafrost-carbon complexities, *Nat. Geosci.*, 6, 675–676,  
851 doi:10.1038/ngeo1937, 2013.
- 852 Vonk, J. E., Mann, P. J., Dowdy, K. L., Davydova, A., Davydov, S. P., Zimov, N., Spencer, R. G. M., Bulygina,  
853 E. B., Eglinton, T. I., and Holmes, R. M.: Dissolved organic carbon loss from Yedoma permafrost amplified  
854 by ice wedge thaw, *Environ. Res. Lett.*, 8, 35023, doi:10.1088/1748-9326/8/3/035023, 2013a.
- 855 Vonk, J. E., Mann, P. J., Davydov, S., Davydova, A., Spencer, R. G. M., Schade, J., Sobczak, W. V., Zimov,  
856 N., Zimov, S., Bulygina, E., Eglinton, T. I., and Holmes, R. M.: High biolability of ancient permafrost carbon  
857 upon thaw, *Geophys. Res. Lett.*, 40, 2689–2693, doi:10.1002/grl.50348, 2013b.
- 858 Vonk, J. E., Tank, S. E., Mann, P. J., Spencer, R. G. M., Treat, C. C., Striegl, R. G., Abbott, B. W., and  
859 Wickland, K. P.: Biodegradability of dissolved organic carbon in permafrost soils and waterways: a meta-  
860 analysis, *Biogeosciences*, 12, 6915–6930, doi:10.5194/bg-12-8353-2015, 2015a.
- 861 Vonk, J. E., Tank, S. E., Bowden, W. B., Laurion, I., Vincent, W. F., Alekseychik, P., Amyot, M., Billet, M. F.,  
862 Canário, J., Cory, R. M., Deshpande, B. N., Helbig, M., Jammot, M., Karlsson, J., Larouche, J., Macmillan,



- 863 G., Rautio, M., Walter Anthony, K. M., and Wickland, K. P.: Reviews and syntheses: Effects of permafrost  
864 thaw on Arctic aquatic ecosystems, *Biogeosciences*, 12, 7129–7167, doi:10.5194/bg-12-7129-2015,  
865 2015b.
- 866 Walsh, J. E., Overland, J. E., Groisman, P. Y., and Rudolf, B.: Snow, Water, Ice and Permafrost in the  
867 Arctic (SWIPA): Climate change and the cryosphere, Arctic Monitoring and Assessment Programme  
868 (AMAP), Oslo, Norway., 2011.
- 869 Ward, R. C. and Robinson, M.: Principles of Hydrology, Fourth Edi., McGraw-Hill International (UK  
870 Limited., 2000.
- 871 Watanabe, S., Laurion, I., Chokmani, K., Pienitz, R., and Vincent, W. F.: Optical diversity of thaw ponds in  
872 discontinuous permafrost: A model system for water color analysis, *J. Geophys. Res. Biogeosciences*,  
873 116, doi:10.1029/2010JG001380, 2011.
- 874 Weishaar, J. and Aiken, G.: Evaluation of specific ultra-violet absorbance as an indicator of the chemical  
875 content of dissolved organic carbon, *Environ. Chem.*, 37, 4702–4708, doi:10.1021/es030360x, 2003.
- 876 Woods, G. C., Simpson, M. J., Pautler, B. G., Lamoureux, S. F., Lafrenière, M. J., and Simpson, A. J.:  
877 Evidence for the enhanced lability of dissolved organic matter following permafrost slope disturbance in  
878 the Canadian High Arctic, *Geochim. Cosmochim. Acta*, 75, 7226–7241, doi:10.1016/j.gca.2011.08.013,  
879 2011.
- 880 Yanagihara, Y., Koike, T., Matsuura, Y., Mori, S., Shibata, H., Satoh, F., Masuyagina, O., Zyryanova, O.,  
881 Prokushkin, A. S., Prokushkin, S. G., and Abaimov, A. P.: Soil respiration on the contrasting north- and  
882 south-facing slopes of a larch forests in Central Siberia, *Eurasian J. For. Res.*, 1, 19–29, 2000.
- 883 Zeileis, A. and Grothendieck, G.: zoo: S3 infrastructure for regular and irregular time series, *J. Stat.*  
884 *Softw.*, 14, 1–27, 2005.
- 885 Zeileis, A. and Hothorn, T.: Diagnostic checking in regression relationships., *R News*, 2, 7–10, 2002.
- 886 Zhou, Y., Guo, H., Lu, H., Mao, R., Zheng, H., and Wang, J.: Analytical methods and application of stable  
887 isotopes in dissolved organic carbon and inorganic carbon in groundwater, *Rapid Commun. Mass*  
888 *Spectrom.*, 29, 1827–1835, doi:10.1002/rcm.7280, 2015.
- 889 Zuur, A. F., Ieno, E. N., Walker, N., Saveliev, A. A., and Smith, G. M.: *Mixed Effects Models and Extensions*  
890 *in Ecology with R*, Springer, New York., 2009.
- 891



892 **Table 1:** Slump characteristics and sampling information for eight retrogressive thaw slumps sampled  
 893 during the 2014 field season on the Peel Plateau, NWT, Canada. Characteristics are derived from  
 894 published values and field estimations.

Slump location	Sample dates (Julian day) <sup>a</sup>	Latitude	Longitude	Scar zone (ha)	Debris tongue (m) <sup>b</sup>	Headwall height (m)
FM4	202, 210, 223	67 16.679	-135 09.573	8.8	960	16 to 20 <sup>d</sup>
FM2	200, 209, 222	67 15.462	-135 14.216	31.7	1529	25 <sup>e</sup>
FM3	197, 212	67 15.100	-135 16.270	6.1	576	10 <sup>e</sup>
SD	196, 213, 234	67 10.818	-135 43.630	3.3	NA	2 – 4 <sup>d</sup>
HA	190, 229	67 09.057	-135 41.121	5.9	288	6 – 10 <sup>d</sup>
HB	190, 229	67 14.397	-135 49.167	13.6 <sup>c</sup>	257	6 – 10 <sup>d</sup>
HC	190, 229	67 19.652	-135 53.620	10.3, 10.3 <sup>c</sup>	408	6 – 10 <sup>d</sup>
HD	190, 229	67 24.025	-135 20.048	1.8	137	6 – 10 <sup>d</sup>
Weather Station		67 14.756	-135 12.920			

895

896 <sup>a</sup> Excludes samples for the FM3 ‘environmental controls’ analysis which was conducted using samples  
 897 from 17 additional dates; HD, Julian date 229 did not include a within-slump sample

898 <sup>b</sup> The length of debris tongue measured from the base of the debris scar, along the valley bottom stream

899 <sup>c</sup> Site HB is comprised of two smaller slump features that have merged into the scar zone delineated  
 900 here; site HC is comprised of 5 separate slump features that have merged into the two scar zones  
 901 delineated here

902 <sup>d</sup> Rough estimates by field crews over 2014 and 2015 field seasons

903 <sup>e</sup> (Kokelj et al., 2015)

904

905

906



907 **Table 2:** Results of the mixed-effects models used to assess the effects of slumping on stream water  
 908 chemistry and optical characteristics. Downstream models incorporated data from downstream and  
 909 upstream sites; within-slump models incorporated data from within-slump and upstream sites. Further  
 910 details on the statistical approach are provided in Section 3.4.  
 911

	Downstream			Within-slump		
	df	t	p	df	t	p
DOC	20	-12.895	<.0001	30	-1.468	0.153
Na	33	9.662	<.0001	30	7.278	0.000
Ca	33	9.767	<.0001	30	4.782	0.000
Mg	33	6.166	<.0001	30	8.593	0.000
Conductivity	32	43.083	<.0001	30	11.895	0.000
TSS	29	6.692	<.0001	28	2.187	0.037
SUVA	31	-5.296	<.0001	30	-35.052	0.000
S <sub>R</sub>	31	5.092	<.0001	31	8.065	0.000
S <sub>275</sub>	30	2.695	0.011	31	8.159	0.000
S <sub>350</sub>	31	-3.595	0.001	31	16.665	0.000

912

913



914 **Table 3:** Measured fraction modern ( $F^{14}C$ ) and estimated calendar years before present for  $^{14}C$  of  
915 dissolved organic carbon samples collected upstream of, and within drainage waters of, selected slump  
916 sites. Data were collected during the summer of 2016. nc indicates sample not collected.

917

Site	$F^{14}C$		$^{14}C$ yr BP	
	Upstream	Within-slump	Upstream	Within-slump
FM4	$0.9734 \pm 0.0029$	nc	$217 \pm 24$	nc
FM2	$0.9764 \pm 0.0032$	$0.3030 \pm 0.0024$	$192 \pm 27$	$9592 \pm 64$
FM3	$1.0023 \pm 0.0030$	$0.3618 \pm 0.0018$	modern	$8167 \pm 39$
SD	$1.0216 \pm 0.0035$	$0.8659 \pm 0.0025$	modern	$1157 \pm 23$



918

919 **Table 4:** Results of multiple linear regression analyses to assess environmental controls on upstream and downstream DOC flux, and upstream  
 920 and downstream DOC concentration. nr indicates variables that were not retained in the best fit regression model; NA indicates variables that  
 921 were not run in individual analyses. Significant p-values are indicated with bold text; marginal results ( $0.05 < p < 0.10$ ) are indicated in italics.  
 922 Model statistics are as follows: downstream flux  $r^2=0.84$ ,  $F_{7,11}=8.25$ ,  $p = 0.001$ ; upstream flux  $r^2=0.87$ ,  $F_{7,11}=10.79$ ,  $p < 0.001$ ; downstream  
 923 concentration  $r^2=0.85$ ,  $F_{4,14}=19.57$ ,  $p < 0.001$ ; upstream concentration  $r^2=0.91$ ,  $F_{5,13}=27.05$ ,  $p < 0.001$ .

Coefficient	Downstream DOC flux			Upstream DOC flux			Downstream DOC concentration			Upstream DOC concentration		
	Estimate	t	p	Estimate	t	p	Estimate	t	p	Estimate	t	p
<b>Average Air Temperature (°C)</b>												
0 h	-67.08	-1.685	0.120	<b>-115.96</b>	<b>-3.286</b>	<b>0.007</b>	nr	nr	nr	<b>0.165</b>	<b>2.349</b>	<b>0.035</b>
48 h	nr	nr	nr	56.32	1.534	0.153	<b>0.332</b>	<b>6.886</b>	<b>&lt;0.001</b>	<b>0.396</b>	<b>5.510</b>	<b>&lt;0.001</b>
72 h	<b>-95.15</b>	<b>-2.594</b>	<b>0.025</b>	<b>-94.17</b>	<b>-2.717</b>	<b>0.020</b>	nr	nr	nr	nr	nr	nr
120 h	nr	nr	nr	nr	nr	nr	<b>0.134</b>	<b>3.527</b>	<b>0.003</b>	<b>0.203</b>	<b>4.411</b>	<b>&lt;0.001</b>
<b>Rainfall (mm)</b>												
0h	<b>116.13</b>	<b>5.411</b>	<b>&lt;0.001</b>	<b>105.47</b>	<b>6.039</b>	<b>&lt;0.001</b>	<i>-0.066</i>	<i>-1.967</i>	<i>0.069</i>	nr	nr	nr
48h	nr	nr	nr	nr	nr	nr	nr	nr	nr	nr	nr	nr
72h	nr	nr	nr	nr	nr	nr	nr	nr	nr	nr	nr	nr
120h	<i>-23.94</i>	<i>-1.970</i>	<i>0.075</i>	<b>-24.15</b>	<b>-2.529</b>	<b>0.028</b>	nr	nr	nr	nr	nr	nr
<b>Average net radiation (W m<sup>-2</sup>)</b>												
0h	4.96	1.286	0.225	nr	nr	nr	<b>-0.021</b>	<b>-4.043</b>	<b>0.001</b>	<b>-0.021</b>	<b>-3.387</b>	<b>0.005</b>
48h	nr	nr	nr	nr	nr	nr	nr	nr	nr	nr	nr	nr
72h	5.58	1.545	0.151	4.04	1.563	0.146	nr	nr	nr	nr	nr	nr
120h	nr	nr	nr	nr	nr	nr	nr	nr	nr	nr	nr	nr
<b>Total suspended sediment (mg L<sup>-1</sup>)</b>												
Downstream	<i>-0.02</i>	<i>-2.102</i>	<i>0.059</i>	NA	NA	NA	nr	nr	nr	NA	NA	NA
Upstream	NA	NA	NA	-0.32	-1.626	0.132	NA	NA	NA	-0.0006	-1.627	0.128

924 **Figure captions:**

925 **Fig. 1:** Panel A depicts the stream networks and location of the eight retrogressive thaw slumps studied  
926 on the Peel Plateau, Northwest Territories, Canada. Panel B depicts representative sampling locations at  
927 each slump site; FM3 depicted. Panels C-E depict representative thaw-slump headwall stratigraphies.  
928 Panel C shows a mega-slump (FM3, the smallest mega-slump, is depicted); panel D shows a moderate-  
929 sized slump (HB); panel E shows the smallest slump that was sampled (SD). In panels C and D, the  
930 approximate location of the modern active layer (a), early Holocene-aged relict active layer (b), and  
931 Pleistocene-aged glacial materials (c) is shown.

932 **Fig. 2:** The effect of retrogressive thaw slumps on stream water dissolved organic carbon (DOC)  
933 concentration. Each data point represents the mean and standard error of measurements across all  
934 sampling dates, as described in Table 1. The bottom two panels show the ratio of within-slump:  
935 upstream, and downstream: upstream DOC concentrations within individual slumps, with points  
936 indicating the mean and standard error of this ratio across sample dates.

937 **Fig. 3:** Box and whisker plots to illustrate the effects of retrogressive thaw slump activity on stream  
938 geochemistry. Each boxplot includes data from across all slumps and sampling periods, and indicates  
939 median values, 25<sup>th</sup> and 75<sup>th</sup> percentiles (box extremities), 10<sup>th</sup> and 90<sup>th</sup> percentiles (whiskers), and  
940 outlier points. U=upstream sites; W=within-slump sites; D=downstream sites.

941 **Fig. 4:** The effect of retrogressive thaw slumps on the **optical properties** of stream water dissolved  
942 organic matter. Each data point represents the mean and standard error of measurements across all  
943 sampling dates, as described in Table 1.

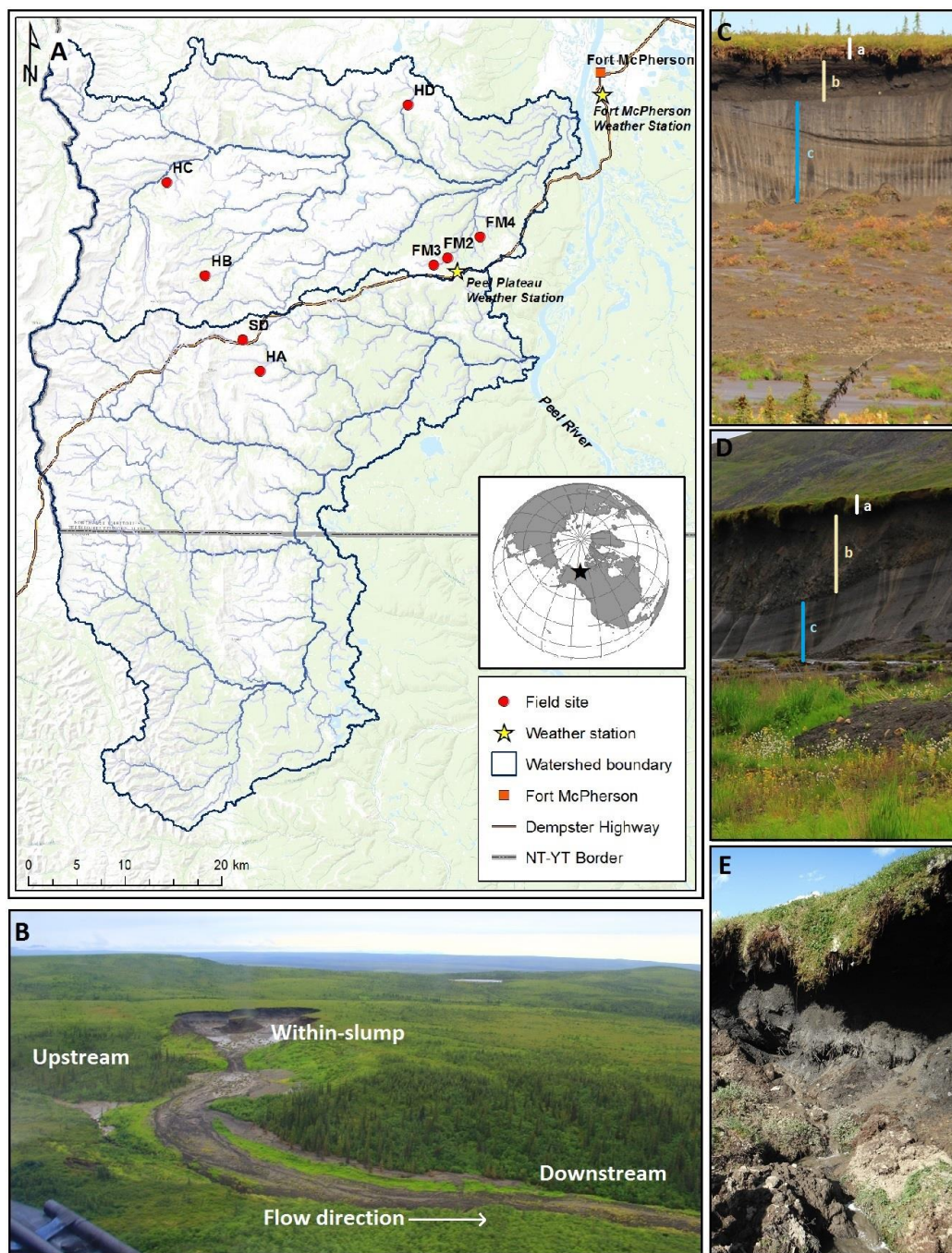
944 **Fig. 5:** Paired data on the oxygen isotopic composition of water ( $\delta^{18}\text{O}$  ‰) and  $\text{SUVA}_{254}$  ( $\text{L mg C}^{-1}\text{m}^{-1}$ )  
945 characteristics of dissolved organic matter (DOM), to demonstrate the relationship between source  
946 water age and DOM composition.  $\delta^{18}\text{O}$  values for the modern active layer, icy diamicton, and  
947 Pleistocene-aged ground ice are from Lacelle et al. (2013): **the modern active layer is equivalent of the**  
948 **meteoric water line**, icy diamicton has been aged to be Holocene era, and the value for Pleistocene-aged  
949 ground ice is the **most enriched Pleistocene-aged** value for this region.

950 **Fig. 6:** Environmental conditions (solar radiation, precipitation and mean daily air temperature) and DOC  
951 flux upstream and downstream of slump FM3 across a month-long sample period (July 12-August 12,  
952 2014). Corresponding multiple linear regressions are described in Table 4.

953 **Fig. 7:** Within-slump fluxes of dissolved organic carbon (DOC), and TSS, compared to the calculated  
954 (downstream - upstream) fluxes for these two constituents. TSS – a conservative tracer over short  
955 distances – shows an additive response where the measured within-slump flux is equivalent to the  
956 calculated (downstream - upstream) flux. In contrast, DOC shows clear evidence of downstream loss.

957

958

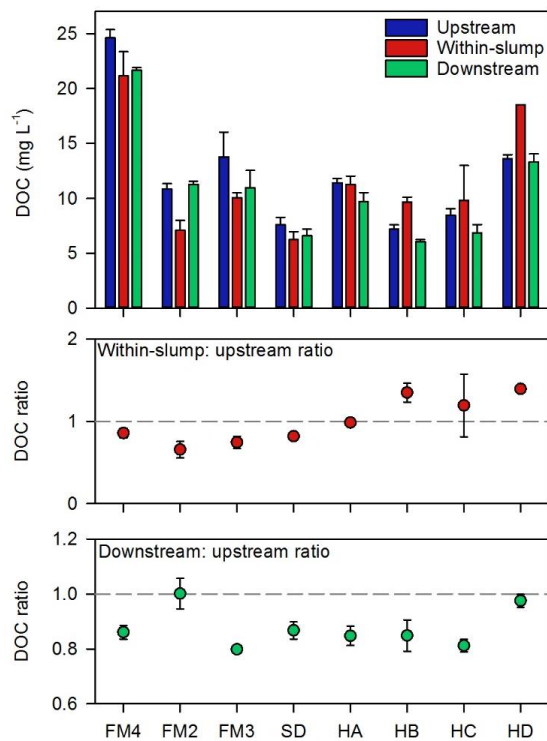


959

960 **Figure 1**



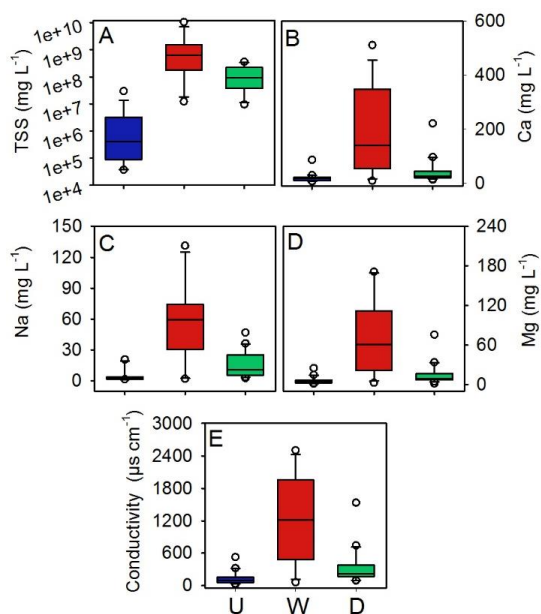
961



962

963 **Figure 2**

964



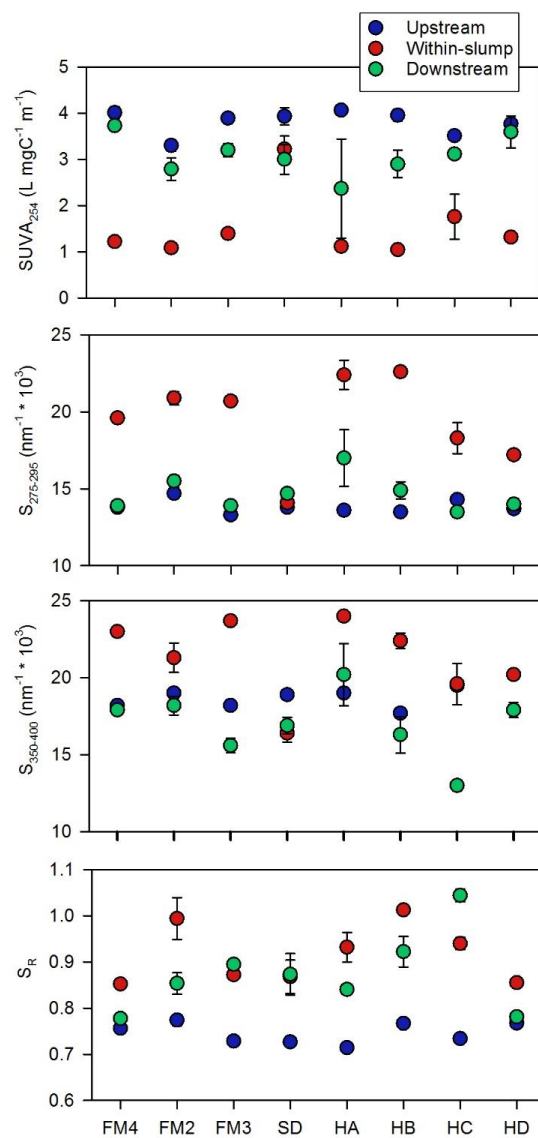
965

966 **Figure 3**

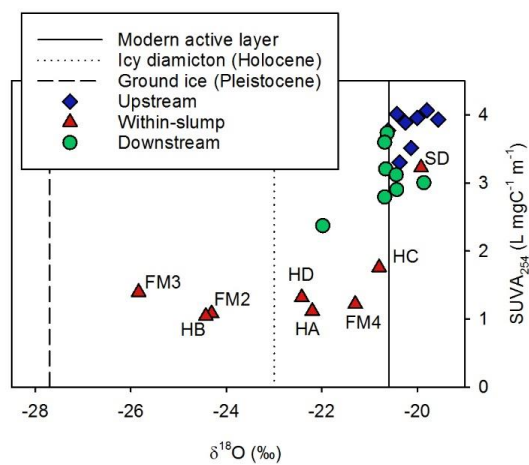
967



968



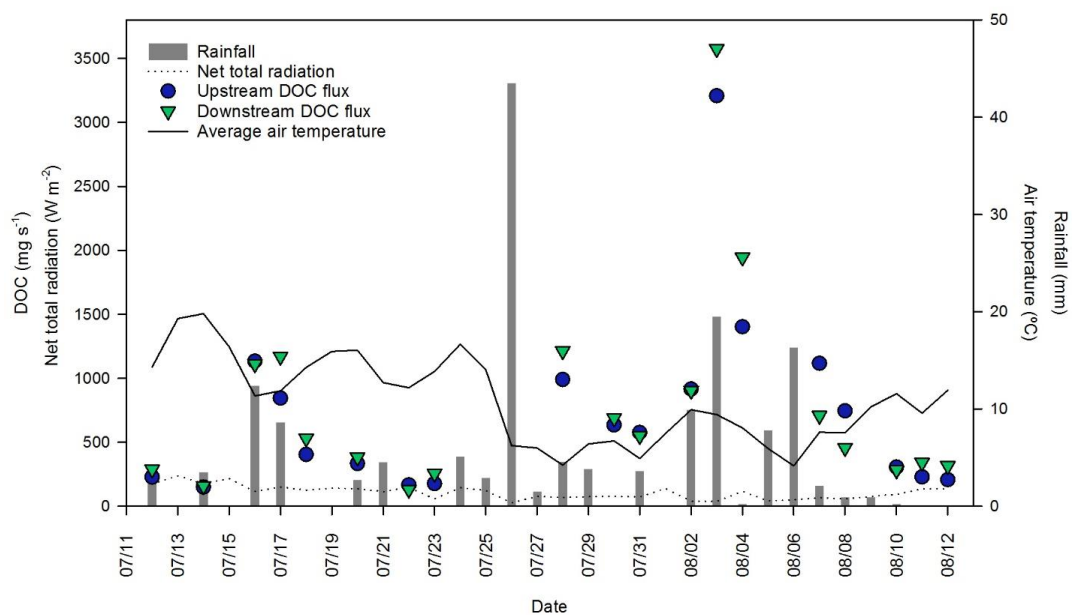
969 **Figure 4**  
 970



971

972 **Figure 5**

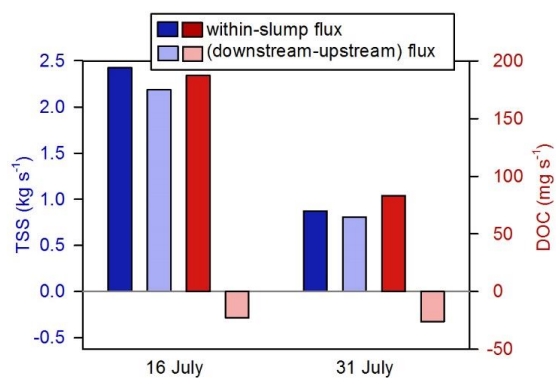
973



974

975 **Figure 6**

976



977

978

979 **Figure 7**